




The pre-induction temperature affects recombinant HuGM-CSF aggregation in thermoinducible *Escherichia coli*

Sara Restrepo-Pineda¹ · Nuria Sánchez-Puig² · Néstor O. Pérez³ · Enrique García-Hernández² · Norma A. Valdez-Cruz¹ · Mauricio A. Trujillo-Roldán^{1,4} 

Received: 2 November 2021 / Revised: 28 March 2022 / Accepted: 30 March 2022 / Published online: 12 April 2022
© The Author(s), under exclusive licence to Springer-Verlag GmbH Germany, part of Springer Nature 2022

Abstract

The overproduction of recombinant proteins in *Escherichia coli* leads to insoluble aggregates of proteins called inclusion bodies (IBs). IBs are considered dynamic entities that harbor high percentages of the recombinant protein, which can be found in different conformational states. The production conditions influence the properties of IBs and recombinant protein recovery and solubilization. The *E. coli* growth in thermoinduced systems is generally carried out at 30 °C and then recombinant protein production at 42 °C. Since the heat shock response in *E. coli* is triggered above 34 °C, the synthesis of heat shock proteins can modify the yields of the recombinant protein and the structural quality of IBs. The objective of this work was to evaluate the effect of different pre-induction temperatures (30 and 34 °C) on the growth of *E. coli* W3110 producing the human granulocyte–macrophage colony-stimulating factor (rHuGM-CSF) and on the IBs structure in a $\lambda pL/pR$ -cI857 thermoinducible system. The recombinant *E. coli* cultures growing at 34 °C showed a ~69% increase in the specific growth rate compared to cultures grown at 30 °C. The amount of rHuGM-CSF in IBs was significantly higher in cultures grown at 34 °C. Main folding chaperones (DnaK and GroEL) were associated with IBs and their co-chaperones (DnaJ and GroES) with the soluble protein fraction. Finally, IBs from cultures that grew at 34 °C had a lower content of amyloid-like structure and were more sensitive to proteolytic degradation than IBs obtained from cultures at 30 °C. Our study presents evidence that increasing the pre-induction temperature in a thermoinduced system allows obtaining higher recombinant protein and reducing amyloid contents of the IBs.

Key Points

- Pre-induction temperature determines inclusion bodies architecture
- In pre-induction (above 34 °C), the heat shock response increases recombinant protein production
- Inclusion bodies at higher pre-induction temperature show a lower amyloid content

Keywords Growth temperature · Recombinant protein · Thermoinduction · Inclusion body · Chaperones, rHuGM-CSF

✉ Mauricio A. Trujillo-Roldán
maurotru@gmail.com; maurotru@biomedicas.unam.mx

¹ Departamento de Biología Molecular y Biotecnología, Instituto de Investigaciones Biomédicas, Universidad Nacional Autónoma de México, Ciudad de México, CP 04510, México

² Universidad Nacional Autónoma de México, Instituto de Química, Ciudad Universitaria, Ciudad de México 04510, México

³ Probiomed S.A. de C.V. Planta Tenancingo, Cruce de Carreteras Acatzingo-Zumpahuacan SN, Tenancingo CP 52400, Estado de México, México

⁴ Departamento de Biología Molecular y Biotecnología, Unidad de Bioprocesos, Instituto de Investigaciones Biomédicas, Universidad Nacional Autónoma de México, Ciudad de México, CP 04510, México

Introduction

The production of recombinant proteins for therapeutic use has become of great interest in current biotechnology and biomedicine. To achieve high product yields, make bio-processes efficient, and minimize production costs, different biological platforms, expression systems, culture medium designs, and purification strategies have been explored (Assenberg et al. 2013; Terol et al. 2021; Kumar et al. 2020; Kaur et al. 2018). *Escherichia coli* as a host for recombinant protein production has numerous advantages compared to other bacteria, yeasts, or mammalian cells (Baeshen et al. 2015; Sánchez-García et al. 2016). *E. coli* can grow on inexpensive substrates in a short time, it is a well-known

organism, high cell density cultures can be easily reached, and the accumulation of the recombinant protein can represent 30% or more of the total cellular protein (Huang et al. 2012; Rosano and Ceccarelli 2014; Rosano et al. 2019). Additionally, within the biopharmaceuticals approved through 2018, ~22% were produced in *E. coli* (Walsh 2018).

When recombinant proteins are overexpressed in *E. coli*, the bacteria tend to form protein aggregates called inclusion bodies (IBs) (Baneyx and Mujacic 2004; Williams et al. 1982). IBs are recombinant protein-enriched deposits with spherical or pseudo-spherical shapes and diameters between 50–800 nm (De Marco et al. 2019; Margreiter et al. 2008; Castellanos-Mendoza et al. 2014). Its formation is a dynamic phenomenon that occurs mainly due to the interactions between partially folded or misfolded polypeptide chains during the overexpression of recombinant proteins, stressful conditions, or the shortage of heat shock proteins (HSPs), which are responsible for maintaining the cell proteome homeostasis (Baneyx and Mujacic 2004; Fahner et al. 2004; Carrió and Villaverde 2003; Hartl and Hayer-Hartl 2009). Although IBs were considered an obstacle in obtaining soluble and active recombinant proteins, recent studies have shown that proteins with native-like structure and polypeptides with amyloid characteristics coexist within IBs, giving them both biological functionality and mechanical stability (González-Montalbán et al. 2007; Cano-Garrido et al. 2013; Rinas et al. 2017; Singhvi et al. 2020). This progress in the perception of IBs has increased the scientific interest in the study of their molecular organization and application in various areas as materials for cell proliferation (García-Fruitós et al. 2010), drug release agents (Villaverde et al. 2012; Pesarrodonna et al. 2019) and biocatalysts (Jäger et al. 2020). Nowadays, it is known that bioprocess conditions such as pH (Castellanos-Mendoza et al. 2014; Calcines-Cruz et al. 2018), temperature (de Groot and Ventura 2006; Peternel et al. 2008; Restrepo-Pineda et al. 2019), agitation (Valdez-Cruz et al. 2017), among others, can determine the formation, composition, and structure of IBs (De Marco et al. 2019). However, the effect of different induction strategies on its properties, for example, the use of a temperature-induced system, is a subject that remains poorly explored.

The $\lambda pL/pR$ -cI857 thermoinducible expression system is a widely applied strategy in the industry to produce recombinant proteins in *E. coli* (Valdez-Cruz et al. 2010, 2011; Restrepo-Pineda et al. 2021). The use of this system avoids the addition of chemical inducers such as isopropyl- β -D-1-thiogalactopyranoside (IPTG), the possibilities of contamination are minimized through the external control of temperature, and target recombinant protein yields of at least 30% can be obtained regarding the total protein (Remaut et al. 1981; Caspeta et al. 2013; Singha et al. 2018). Below 37 °C, recombinant protein expression is regulated by the binding of the cI857 thermolabile repressor to the operator regions

of the pL and pR promoters derived from bacteriophage λ , facilitating the formation of a DNA loop that inhibits RNA polymerase activity (Dodd et al. 2004; Lewis et al. 2016). By raising to 37 °C, cI857 is released and allows the transcription of the gene of interest (Caulcott and Rhodes 1986; Villaverde et al. 1993; Valdez-Cruz et al. 2010). However, it has been reported that above 34 °C, *E. coli* initiates the heat shock response (HSR) to cope with heat stress and maintain cellular homeostasis (Yamamori et al. 1978; Morita et al. 1999; Yano et al. 1990; Yura 2019). HSR is controlled by the transcription factor σ^{32} (RpoH), which regulates the expression of an extensive network of chaperones and proteases involved in folding of nascent proteins and the removal of damaged/unfolded proteins (Guisbert et al. 2004, 2008; Baneyx and Mujacic 2004; Balchin et al. 2016). The temperature upshift during recombinant protein synthesis also involves a metabolic adaptation, reflected in the reduction of the specific growth rate, accumulation of organic acids, mainly acetate, and a readjustment in metabolic fluxes (Hoffmann and Rinas 2004; Hoffman et al. 2002; Wittmann et al. 2007; Restrepo-Pineda et al. 2021). Recombinant protein production typically follows a two-phase strategy; initially, cells are grown at 30 °C (in batch or feed-batch cultures), and then recombinant protein expression is induced at a constant temperature between 38 °C and 42 °C (Caspeta et al. 2009, 2013; Valdez-Cruz et al. 2010; Restrepo-Pineda et al. 2021).

In a thermoinduced system in addition to HSR, recombinant protein overexpression and the IBs formation co-occur (Valdez-Cruz et al. 2010, 2011; Restrepo-Pineda et al. 2021). Also, HSPs are overexpressed in response to elevated temperature and recombinant protein accumulation (Gill et al. 2000; Carrió and Villaverde 2003). During thermoinduction, the mRNA levels of heat shock genes (*dnaK*, *dnaJ*, and *groEL*) increase between 2 and 9 times compared with 30 °C (Valdez-Cruz et al. 2011). At the proteomic level, Hoffmann and Rinas (2000) found that just 30 min after thermoinduction at 42 °C, HSPs reach their maximum synthesis rate, and IBs analyzed one-hour post-induction contains chaperones such as DnaK, GroEL, IbpA, and IbpB. Previous findings in our laboratory revealed that using a thermoinducible system, GroEL is present in both the soluble protein fraction and in the IBs. At the same time, DnaK predominated in the soluble fraction (Restrepo-Pineda et al. 2019). The presence of these chaperones in IBs has been related to their function in the dissolution of these aggregates or preventing their aggregation during thermoinduction (Rinas et al. 2007). Moreover, the assembly and morphology of IBs can also be modified depending on the absence or presence of specific HSPs (García-Fruitós et al. 2010). Furthermore, IBs harvested from *E. coli* cultures induced by IPTG at high temperatures (39 or 42 °C) were more accessible to be solubilized in urea than those obtained at lower temperatures (20 and 30 °C) (Singh et al. 2020).

Granulocyte–macrophage colony-stimulating factor (GM-CSF) is a protein whose primary function is to stimulate germinal hematopoietic cells for the formation of the differentiated myeloid lineage and takes part in regulating a wide variety of inflammatory responses (Francisco-Cruz et al. 2014; Wicks and Roberts 2016; Hamilton 2019; Dougan et al. 2019). GM-CSF has been recombinantly expressed in mammalian cells, yeasts, and bacteria, receiving FDA (Food and Drug Administration) approval in 1991 for the treatment of neutropenia (Mehta et al. 2015; Dougan et al. 2019). Even though the human GM-CSF contains *O*- and *N*-glycosylation sites (Walter et al. 1992), the non-glycosylated form produced in *E. coli* is biologically active and has therapeutic relevance (Okamoto et al. 1991; Cumming 1991). Recent studies have elucidated the protective role of GM-CSF in autoimmune diseases such as pulmonary alveolar proteinosis (Trapnell et al. 2020; Zhang et al. 2020), its use in oncolytic immunotherapies, and adjuvant in cancer vaccines (Kaufman et al. 2014) as well as its possible administration in treatments against COVID-19 (Lang et al. 2020; Bonaventura et al. 2020).

Although some studies revealed the influence of induction temperature and induction time on IBs structure using a thermoinducible system (Caspeta et al. 2009, 2013; Restrepo-Pineda et al. 2019), this report aimed to elucidate the effect of growth (or pre-induction) temperature on the subsequent formation process, protein composition and structural characteristics of IBs from an *E. coli* bacterial culture producing the recombinant human GM-CSF (rHuGM-CSF). Here, bioreactor cultures of *E. coli* W3110 grown at either 30 or 34 °C were subsequently thermoinduced at 42 °C. Growth curves, carbon source consumption, and acetate production were analyzed. SDS-PAGE evaluated the expression kinetics of the rHuGM-CSF protein in the total protein fraction and IBs. Changes in the expression of some HSPs (DnaK/J, GroEL/ES) were identified by western blot. The structural analysis of the aggregates was carried out using attenuated total reflection-Fourier transform infrared spectroscopy (ATR-FTIR), binding to an amyloidogenic dye, proteolytic digestion, and denaturation with a chaotropic agent. Finally, the secondary structure of the refolded and purified rHuGM-CSF from IBs was studied by circular dichroism (CD) to elucidate its biological activity indirectly.

Materials and methods

Strain, media composition, and bioreactor conditions

E. coli W3110 (ATCC® 27325™) was used as a host to produce the recombinant human granulocyte–macrophage colony-stimulating factor (rHuGM-CSF). The coding

sequence for the rHuGM-CSF (GenBank accession number OL419360) was cloned in the pV3 plasmid containing the gene of the cI857 thermolabile repressor and the *pL* promoter from bacteriophage λ (Lowman and Bina 1990). pV3 is a low copy number plasmid based on the RepA-CopB from R100 plasmid (Olsson et al. 2004) and the *par* sequence to increase plasmid stability from plasmid pSD101 (Miller et al. 1983). A working cell bank containing aliquots of 1 ml at an optical density at 600 nm (OD_{600}) of 1.09 absorbance units (AU) was generated with 40% (v/v) glycerol and stored at -75 °C (Restrepo-Pineda et al. 2019).

For inoculums and bioreactor cultures, a defined culture medium was prepared as described in Restrepo-Pineda et al. (2019), as follows (in g/l): 4.0 (NH₄)₂HPO₄; 13.3 KH₂PO₄; 1.7 citric acid; 1.2 MgSO₄·7H₂O; 0.045 thiamine; 0.1 kanamycin; 17.5 glucose; 3.0 casamino acids and trace elements (2.0 ml/l of 500X stock). Glucose, MgSO₄, and trace elements stocks were separately sterilized at 121 °C and 22 *psig* for 30 min (ES-215 sterilizer, Tomy Digital Biology, Tokyo, Japan). Thiamine, casamino acids, and kanamycin solutions were sterilized using 0.22- μ m-pore-size filters (Merck Millipore, Billerica, MA, USA) and added before inoculation. The pH of the culture medium was adjusted to 7.0 \pm 0.1 with 3 N NaOH and 8 N HCl.

For preparing the inoculum, 500 μ l of the working cell bank was cultured in conventional 250-ml Erlenmeyer flasks with 50 ml filling volume. Cells were incubated overnight (~14 h) at 30 °C and 200 rpm (New Brunswick Scientific Classic C25, Enfield, CT, USA). The inoculum volume was decided based on the OD_{600} measurement to start the bioreactor experiments with the same cell concentration (~0.1 AU). The batch cultures were carried out in 1.2-l bioreactors (Applikon, Delft, Netherlands) with a working volume of 800 ml. Dissolved oxygen tension (DOT) was controlled at 35% with respect to air saturation by a cascade of agitation between 100–1000 rpm and constant airflow rate (1 vvm, volume of air per volume of culture medium). Medium pH in bioreactors was maintained at 7.0 \pm 0.1 by adding 3 N NaOH or 3 N HCl. The temperature was controlled to either 30 or 34 °C (42 °C for induction) using a heating/cooling circulating water bath (PolyScience, Niles, IL, USA). To avoid foaming, a sterile antifoam agent was added manually when necessary. pH, DOT, and temperature were monitored and controlled online with the BioXpert software (Applikon, Delft, Netherlands).

Cell concentration estimation

Growth of the strain *E. coli* W3110 producing rHuGM-CSF was determined by following the OD_{600} (Spectronic Genesys 5, Thermo Electron Corporation, Westmont, IL, USA). OD_{600} measurements were converted to dry cell weight (DCW) through a linear correlation standard curve.

Briefly, 10 ml samples from three independent cultures were centrifuged at $8,000\times g$ for 10 min. The cell pellet was washed with 1X PBS (pH 7.5) twice and filtered using 0.22- μm -pore-size filters (Merck Millipore, Billerica, MA, USA). The wet cell paste was dried at $90\text{ }^\circ\text{C}$ for 48 h. After complete drying, the filters were weighed again. The difference in mass was used to calculate the DCW. 1.0 AU was equivalent to $0.33\pm 0.04\text{ g/l}$ of DCW.

Recombinant protein thermoinduction

Bioreactor cultures were grown at either 30 or $34\text{ }^\circ\text{C}$ until reaching the pre-stationary phase (OD_{600} of 2.0–3.0 AU). At this point, the thermoinduction of rHuGM-CSF production was carried out by increasing to $42\text{ }^\circ\text{C}$, maintaining DOT and pH control (Restrepo-Pineda et al. 2019). The heating rate was the same in both conditions ($0.5\text{ }^\circ\text{C}/\text{min}$). Samples of 1.0 ml were taken at different post-induction times (1, 3, 5, 10, and 18/20 h) and centrifuged at $10,000\times g$ for 10 min. Supernatants were used for glucose and acetate estimation, while pellets were stored at $-20\text{ }^\circ\text{C}$ for further analysis. All experiments were performed in triplicate.

Glucose and acetate quantification

Supernatants were filtered using sterile syringe filters with a 0.22- μm -pore-size before injection. Glucose concentration was determined in a biochemistry analyzer YSI 2900D (YSI Inc, Yellow Springs, OH, USA) equipped with a glucose oxidase membrane (YSI 2365), a buffer solution (YSI 237), and a standard calibrator solution (2.5 g/l of glucose). The concentrations of acetate were determined by high-performance liquid chromatography (HPLC) in a Shimadzu LC-20AT (Shimadzu, Kyoto, Japan) using an Aminex HPX-87H column (300 \times 7.8 mm; 9- μm internal diameter, Bio-Rad, Hercules, CA, USA). The mobile phase consisted of 0.008 N NH_2SO_4 with 0.6 ml/min at $50\text{ }^\circ\text{C}$ and 215 nm UV absorbance. A commercial standard solution was used for acetate (No. 125–0586, Bio-Rad), and data obtained were processed in the LC Solution software (Shimadzu, Kyoto, Japan).

Recovery and purification of IBs

For IBs isolation, the method described in Calcines-Cruz et al. (2018) was followed with minor modifications. Briefly, the cell biomass pellets from 1 ml culture were diluted in lysis buffer (50 mM Tris-HCl, 100 mM NaCl, 1 mM EDTA, pH 7.5) containing protease inhibitor (0.1 mM PMSF, phenylmethylsulfonyl fluoride). Each sample was disrupted by sonication using a Soniprep150 (Sanyo Gallenkamp PLC, Loughborough, UK) at 8 μm amplitude in 3–10 cycles of 30 s, keeping on ice. The lysed cell mixture was centrifuged at $14,000\times g$ for 15 min at $4\text{ }^\circ\text{C}$, and both the supernatant

with the total soluble protein and the pellet with the insoluble protein (IBs) were recovered. Insoluble protein fraction was incubated in lysis buffer with 1% (v/v) IGEPAL (Sigma Aldrich, St. Louis, MO, USA) for 30 min under agitation at $4\text{ }^\circ\text{C}$ and centrifuged at $14,000\times g$ for 5 min. The pellet was resuspended in lysis buffer containing 0.5% (v/v) Triton X-100 and centrifuged at $14,000\times g$ for 15 min. Finally, the pellet was washed 3 to 5 times with deionized water, centrifuged between each wash ($14,000\times g$ for 15 min), and the purified IBs were stored at $-20\text{ }^\circ\text{C}$.

Protein quantification, rHuGM-CSF identification, and chaperones immunodetection

The concentration of total soluble protein and protein in the IBs was measured by Bradford assay (Bio-Rad, Hercules, California, USA) according to supplier recommendations. Insoluble proteins were previously solubilized in isoelectric focusing (IEF) buffer (final 1:5 dilution) at room temperature for at least 3 h. Calibration curves with bovine serum albumin (BSA, Equitech-Bio, Kerrville, TX, USA) were made. Both samples and standards were prepared in triplicate, and OD_{600} was measured on a Stat Fax 2100 Microplate Reader (Awareness Technology Inc., Palm City, FL, USA).

Samples collected were used to analyze the production of the total soluble protein and rHuGM-CSF accumulation in IBs on 15% sodium dodecyl sulfate–polyacrylamide gel electrophoresis (SDS-PAGE). Previously, equal amounts of protein were solubilized using 2.5% SDS for 12 h at room temperature, and 20 μg of protein was loaded in each lane. Gels were stained with Coomassie Brilliant Blue R-250 (Bio-Rad, Hercules, CA, USA), and the percentage of rHuGM-CSF in IBs was determined by densitometry using the Image-Lab software and Gel Doc EZ Imager (Bio-Rad, Hercules, CA, USA).

The specific detection of chaperones was carried out by western blot, as reported by Restrepo-Pineda et al. (2019). Proteins in the polyacrylamide gels were transferred to a polyvinylidene difluoride (PVDF) membrane (Immobilon, Millipore, Bedford, MA, USA) by a semi-wet approach via Trans-Blot system (Bio-Rad, Hercules, California, USA). Membranes were blocked for 40 min with 1X TBS plus 5% skim-milk at room temperature and gentle shaking. Two washes for 10 min each were made with wash buffer (1X TBS plus 0.06% Tween-20), and primary antibodies (mouse DnaK ADI-SPA-880 dilution 1:7500, rabbit GroEL ADI-SPA-875 dilution 1:7500, rabbit DnaJ ADI-SPA-410 dilution 1:2000, and rabbit GroES ADI-SPA-210 dilution 1:7500; Enzo Life Sciences, Farmingdale, NY, USA) were added for 1 h at room temperature. Later, membranes were washed three times, followed by incubation with the corresponding secondary antibodies (goat anti-mouse IgG A9044 dilution 1:2500 and goat anti-rabbit IgG A0545

dilution 1:2500, HRP-conjugated, Merck-Sigma-Aldrich, St. Louis, MI, USA) for 1 h at room temperature. Three more washes were done, and the proteins were detected by chemiluminescence using SuperSignal West Pico and Femto substrates (Thermo Fisher Scientific, Waltham, MA, USA) in a C-DIGIT blot scanner (LI-COR, Lincoln, NE, USA). A homemade chemiluminescence marker was used to reveal the images, and the membranes were incubated with mild stripping buffer (glycine, SDS, Tween-20, pH 2.2) to remove the antibodies.

ATR-FTIR spectroscopy

The components of the secondary structure of IBs were identified by attenuated total reflection (ATR)–Fourier transform infrared (FTIR) spectroscopy (Valdez-Cruz et al. 2017; Calcines-Cruz et al. 2018; Singh et al. 2020; Gil-Garcia et al. 2020). Freshly purified IBs were dried at room temperature for 1 h using a speed vacuum concentrator and placed on Specac Quest ATR diamond accessory (Specac Limited, Slough, UK) coupled to an infrared spectrometer IRAffinity-1S (Shimadzu, Kyoto, Japan). Each sample consisted of 40 acquisitions with a resolution of 2 cm^{-1} in the range of $1500\text{--}1700\text{ cm}^{-1}$ and subsequently averaged. After 13 points of smoothing, the second derivatives of the spectrum of the amide I region were determined with the IR LabSolutions program (Shimadzu, Kyoto, Japan) and normalized with respect to the absolute value of the tyrosine peak ($\sim 1508\text{ cm}^{-1}$) (Ami et al. 2005). The analysis of the location frequencies indicated the abundance of the different elements of the secondary structure in the IBs.

Thioflavin T binding assay

The amyloidogenic properties of IBs were evaluated by measuring the fluorescence after binding to the thioflavin T (Th-T) dye (Castellanos-Mendoza et al. 2014; Calcines-Cruz et al. 2018; Singh et al. 2020; Gil-Garcia et al. 2020). 50 mg/ml of protein in IBs were resuspended in phosphate buffer (pH 7.5) containing $75\text{ }\mu\text{M}$ of Th-T (Sigma Aldrich, St. Louis, MO, USA) and incubated for 1 h at $25\text{ }^\circ\text{C}$. The fluorescence signal was measured in a Cary Eclipse Fluorescence Spectrophotometer (Agilent Technologies, Palo Alto, CA, USA) with an excitation wavelength of 440 nm and 5 nm bandwidth. The emission spectrum was recorded from 450 to 560 nm with a spectral resolution of 5 nm. Each spectrum was acquired five times, averaged, and smoothed. The spectrum of Th-T without protein was obtained as a control.

Proteinase K digestion

The resistance of the IBs to enzymatic degradation was determined by incubating 50 mg/ml of sample with $25\text{ }\mu\text{g/ml}$

of proteinase K (PK, Sigma Aldrich, St. Louis, MO, USA). The proteolytic digestion was carried out in 1 ml of buffer (50 mM Tris–HCl and 150 mM NaCl, pH 8.0) at room temperature. Changes in absorbance were monitored at 350 nm for 100 min in a UV/Vis DU@730 spectrophotometer (Beckman Coulter Inc., Brea, CA, USA) mixing by pipetting every minute. Data were normalized with respect to the initial absorbance value (Upadhyay et al. 2012; Castellanos-Mendoza et al. 2014; Valdez-Cruz et al. 2017; Calcines-Cruz et al. 2018; Singh et al. 2020).

Stability in guanidinium chloride

The stability of IBs against chemical solubilization was examined by adding 1.0 mg/ml of protein in IBs to 100 μl of 10 mM Tris–HCl buffer (pH 7.5) containing different concentrations (0, 1, 3 and 5 M) of guanidinium hydrochloride (GndHCl, Sigma-Aldrich, St. Louis, MO, USA). After 24 h of gentle shaking at room temperature, the samples were centrifuged at $8000\times g$ for 10 min. The supernatants were recovered, and the solubilized protein was quantified by the Bradford method described above. The solubility profiles of the IBs harvested at different times after induction were obtained by plotting the soluble protein concentration against GndHCl concentration (De Groot and Ventura 2006; Espargaró et al. 2008; Castellanos-Mendoza et al. 2014).

IBs solubilization, refolding, and purification of rhGM-CSF

Purified IBs of rHuGM-CSF were resuspended in a solubilization buffer (6 M GndHCl, 50 mM 2-mercaptoethanol in 100 mM Tris base, pH 8.2, adjusted with 3 M HCl) at 700 rpm, 1 h and $25\text{ }^\circ\text{C}$ to a final protein concentration of 1.0 mg/ml. Then, the protein folding process was carried out at $25\text{ }^\circ\text{C}$, 100 rpm, and 4 h by drop-by-drop dilution (1:10) of the solubilized product in a Tris base buffer (20 mM , pH 8.2). The reaction was stopped by adding 4 M acetic acid to a final concentration of 0.2 M (Burgess et al. 1987; Belew et al. 1994; Thomson et al. 2012).

The folded protein solution was purified by reverse-phase HPLC in a Shimadzu LC-20AT (Shimadzu, Kyoto, Japan) using a Zorbax Eclipse XDB-C8 column (Agilent Technologies, Santa Clara, CA, USA). A standard curve of the European Pharmacopoeia reference standard for human GM-CSF (Molgramostim, Y0000251, Sigma Aldrich, St. Louis, MO, USA) was carried out at 1.345 mg/ml, 0.672 mg/ml, and 0.336 mg/ml. The folded protein sample ($\sim 10\text{ }\mu\text{g}$) was loaded in the HPLC at $50\text{ }^\circ\text{C}$ with a detector wavelength of 214 nm and a maximum column pressure of 3000 psig . Solutions of 0.1% v/v trifluoroacetic acid (TFA) in water (mobile phase A) and 0.1% v/v TFA in 90% acetonitrile (mobile

phase B) were used for the linear gradient elution at a flow rate of 1.2 ml/min (Nicola et al. 1983; Das et al. 2011).

Circular dichroism (CD) spectroscopy

CD spectra of purified rHuGM-CSF in water were recorded at 37 °C in the far-UV region with a JASCO J-720 spectropolarimeter (Jasco Inc., Easton, MD) described elsewhere (Luviano et al. 2019). Protein solutions of ~0.05 mg/ml were loaded into a quartz cell of 0.1-cm length path. Each spectrum corresponded to the average of three repetitive scans and was corrected by the buffer signal. Ellipticities are reported as mean residue ellipticity, $[\theta]_{\text{mrw}}$. Secondary structure content was calculated from CD spectra using the deconvolution software K2D3 (Louis-Jeune et al. 2012).

Statistical analysis

Statistically significant differences between the data were calculated using analysis of variance (ANOVA), followed by Tukey's test. The quantitative results are expressed as mean \pm standard error of the mean. A p -value < 0.05 was considered statistically significant.

Results

Pre-induction temperature affects the specific growth rate (μ) in thermoinduced *E. coli* cultures.

Cultures of *E. coli* W3110 were grown at either 30 or 34 °C until reaching the pre-stationary phase of growth (OD_{600} nm of 2.0–3.0 AU). Thermoinduction (at 42 °C with a heating rate of 0.50 °C/min) was done in the pre-stationary phase to have a large number of viable cells and take advantage of the fact that the stress responses associated with entering the stationary phase, due to nutrients limitation or the presence of secondary metabolites, has not been triggered (Hengge-Aronis, 1993; Overton, 2014). The dry cell weight (DCW) determination indicated that 1.0 AU was equivalent to 0.33 ± 0.04 g/l of DCW, similar to that reported in other works: 0.32 g/l for recombinant *E. coli* W3110 (Sandoval-Basurto et al. 2004); 0.31 ± 0.05 g/l for recombinant *E. coli* 53,606 (Restrepo-Pineda et al. 2019) and 0.28 g/l for a recombinant strain derived from *E. coli* K-12 (Mansey et al. 2014). Figure 1 compares the kinetics of biomass, the consumption of the carbon source, and the production of acetate. The maximum biomass (X_{max}) for the cultures grown at 30 °C \rightarrow 42 °C was 3.48 ± 0.19 g/l at 21 h (Fig. 1A, Table 1) and for those grown at 34 °C \rightarrow 42 °C was 3.48 ± 0.31 g/l at 15 h (Fig. 1B, Table 1).

A significant difference in the specific growth rate (μ) before thermoinduction is observed between cultures of

30 °C \rightarrow 42 °C (0.53 ± 0.01 h⁻¹) and cultures of 34 °C \rightarrow 42 °C (0.90 ± 0.07 h⁻¹) as shown in Table 1. This represents an increase of ~69% in the μ of recombinant *E. coli* growing at a higher temperature (34 °C). Glucose was consumed entirely in both cases, reaching values close to zero after 20 h of culture (Fig. 1C, D). Interestingly, no significant differences were observed in the biomass per glucose yield ($Y_{X/S}$) and the acetate per biomass yield ($Y_{AC/X}$) between cultures with different pre-induction temperatures (30 and 34 °C; Table 1). However, cultures growing at 34 °C \rightarrow 42 °C consumed the carbon source faster, yielding a specific glucose consumption rate (q_s) of 3.74 ± 0.34 g/g·h, which is 1.5 higher than for cultures grown at 30 °C \rightarrow 42 °C with q_s of 2.64 ± 0.20 g/g·h (Table 1). Similarly, the specific acetate production rate (q_p) was ~65% higher in the cultures at 34 °C \rightarrow 42 °C than at 30 °C \rightarrow 42 °C (Table 1). Acetate reached similar maximum concentrations of 6.58 ± 0.39 g/l at 30 °C \rightarrow 42 °C and 6.38 ± 0.63 g/l at 34 °C \rightarrow 42 °C after 17 h of culture (Fig. 1E, F).

The DOT was controlled in the bioreactors through a proportional–integral–derivative (PID) control algorithm (Trujillo-Roldán et al. 2001). DOT oscillated around the setpoint of 35%, confirming no oxygen limitation in the cultures (Supplemental Fig. S1A, B). Likewise, the pH of the medium was kept close to 7.0 ± 0.1 using an automatic addition system of 3 N NaOH or 3 N HCl (Supplemental Fig. S1C, D).

rHuGM-CSF is preferentially accumulated in IBs using a thermoinducible system, and the amount of recombinant protein within IBs increased to 34 °C \rightarrow 42 °C

To determine the amount of rHuGM-CSF produced after thermoinduction, fractions of total protein obtained from cultures growing at either 30 °C \rightarrow 42 °C or 34 °C \rightarrow 42 °C were analyzed on 15% SDS-PAGE (Supplemental Fig. S2). Samples of different post-induction times (1, 3, 5, and 18/20 h) were loaded in gels, and a sample before thermoinduction (0 h) was used as a negative control. A band corresponding to the molecular weight of the rHuGM-CSF protein (~14–15 kDa) was seen after thermoinduction for both conditions (Supplemental Fig. S2). The densitometric analysis of the gel 1 h after thermoinduction revealed that rHuGM-CSF corresponds to ~22% of the total protein for the 34 °C \rightarrow 42 °C cultures (Supplemental Fig. S2B), while for the 30 °C \rightarrow 42 °C cultures, rHuGM-CSF band represented ~11.5% of the total protein (Supplemental Fig. S2A). The amounts of recombinant protein increased with the induction time, reaching at the end of the culture percentages of ~34% of rHuGM-CSF at 30 °C \rightarrow 42 °C and ~30% of rHuGM-CSF at 34 °C \rightarrow 42 °C (Supplemental Fig. S2).

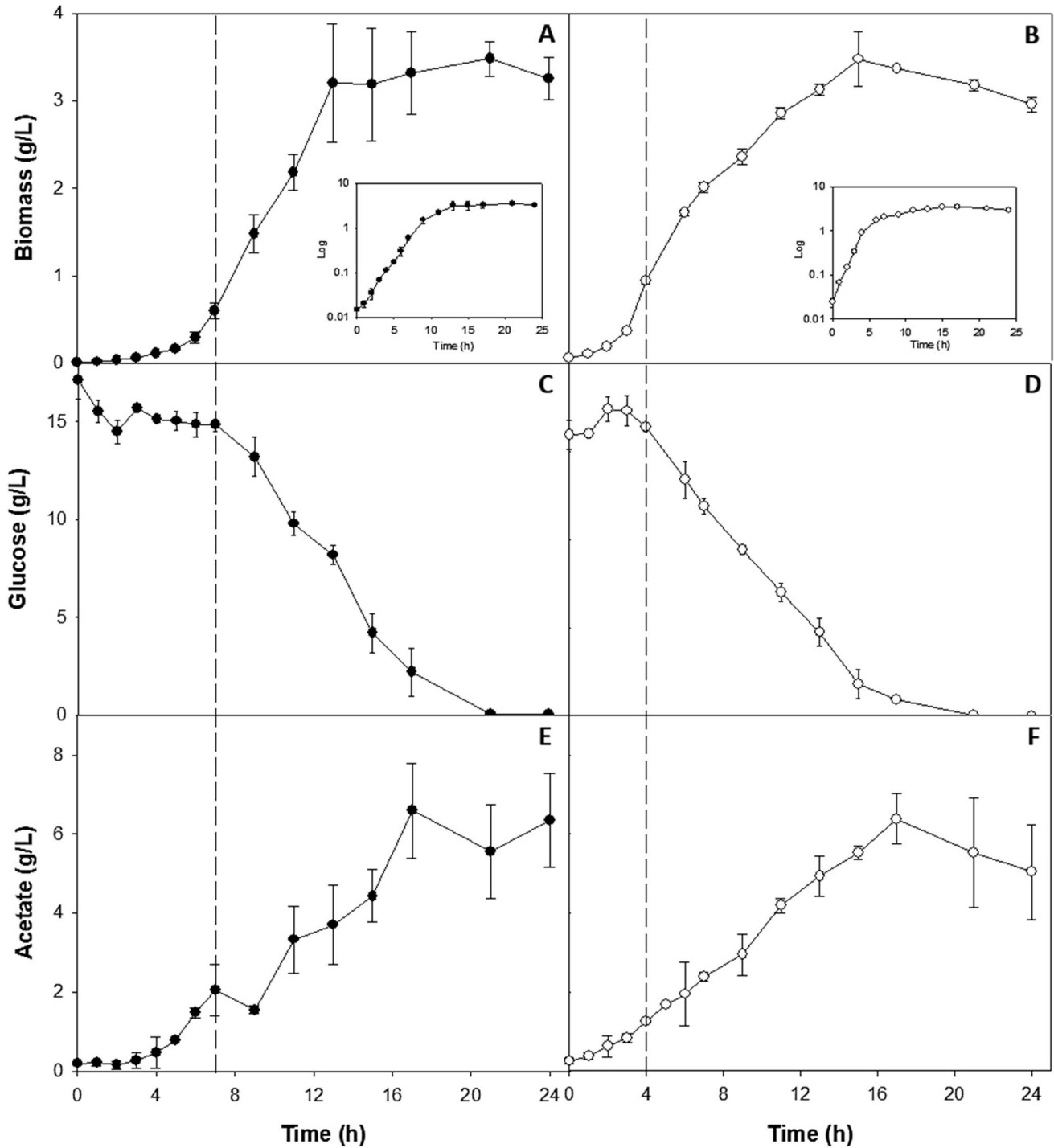


Fig. 1 Kinetics of bacterial growth (A, B), glucose consumption (C, D), and acetate production (E, F) of *E. coli* W3110 producing the rHuGM-CSF protein in 1.2-l bioreactors. Two pre-induction temperatures were evaluated: 30 °C (filled circles) and 34 °C (open circles) with subsequent thermoinduction at 42 °C. Vertical dotted lines indi-

cate the start of the temperature increase (7 h for 30 °C and 4 h for 34 °C), which correspond to an OD_{600} of ~2.0 AU. The graph presents the mean with their respective standard deviation of three independent experiments

Similar final concentrations of 0.34 ± 0.10 g/l at 30 °C → 42 °C and 0.26 ± 0.04 g/l at 34 °C → 42 °C of rHuGM-CSF were obtained (Table 1). Our results agree with previous

reports, where recombinant protein yields close to 30% of the total protein were achieved in a thermoinducible expression system (Remaut et al. 1981; Valdez-Cruz et al. 2010).

Table 1 Comparison of the kinetic parameters of *E. coli* W3110 bioreactor cultures growing at two different temperatures: 30 °C and 34 °C with subsequent thermoinduction of rHuGM-CSF at 42 °C. The mean and standard deviation of three biological replicates per condition are presented

	Growth at 30 °C Induction at 42 °C		Growth at 34 °C Induction at 42 °C	
	Before induction	After induction	Before induction	After induction
^A μ (h ⁻¹)	0.53 ± 0.01 ^a	0.14 ± 0.03 ^b	0.90 ± 0.07 ^c	0.11 ± 0.01 ^b
^B td (h)		1.30 ± 0.03 ^a		0.78 ± 0.08 ^b
^B X_{max} (g _{DCW} /L)		3.48 ± 0.19 ^a		3.48 ± 0.31 ^a
^C $Y_{\text{X/S}}$ (g _{DCW} /g _{GLC})		0.20 ± 0.02 ^a		0.25 ± 0.03 ^a
^D q_s (g _{GLC} /g _{DCW} ·h)		2.64 ± 0.20 ^a		3.74 ± 0.34 ^b
^E $Y_{\text{AC/X}}$ (g _{AC} /g _{DCW})		1.61 ± 0.76 ^a		1.56 ± 0.20 ^a
^F q_p (g _{AC} /g _{DCW} ·h)		0.86 ± 0.41 ^a		1.41 ± 0.20 ^b
Total protein, TP (g/l)		1.01 ± 0.10 ^a		0.85 ± 0.03 ^b
^G rHuGM-CSF in TP (%)		34 ± 3 ^a		30 ± 4 ^a
rHuGM-CSF in TP (g/l)		0.34 ± 0.10 ^a		0.26 ± 0.04 ^a
^H $Y_{\text{TP/X}}$ (g _{TP} /g _{DCW})		0.29 ± 0.08 ^a		0.24 ± 0.05 ^a
^I rHuGM-CSF in IBs (%)		45 ± 2 ^a		53 ± 3 ^b
^J $Y_{\text{RP/X}}$ (g _{RP} /g _{DCW})		0.06 ± 0.03 ^a		0.12 ± 0.02 ^b

Abbreviations: μ , specific growth rate; td : doubling time; X_{max} , maximum biomass concentration; DCW, dry cell weight; GLC, glucose; AC, acetate; $Y_{\text{X/S}}$, biomass per substrate yield; $Y_{\text{AC/X}}$, acetate per biomass yield; q_s , specific glucose consumption rate; q_p , specific acetate formation rate; TP, total protein; IBs, inclusion bodies; RP, recombinant protein; $Y_{\text{TP/X}}$, total protein per biomass yield; $Y_{\text{RP/X}}$, rHuGM-CSF per biomass yield; rHuGM-CSF, recombinant human granulocyte–macrophage colony-stimulating factor

Data are presented as mean ± standard deviation

A non-statistically significant test result ($P > .05$) is represented with the same letter, and a statistically significant test result ($P < .05$) is represented with a different note

A: μ after induction was calculated from cell growth just after thermoinduction until the beginning of steady state

B: X_{max} was reached at 21 h in cultures grown at 30 °C and 15 h in cultures grown at 34 °C

C, E: $Y_{\text{X/S}}$ and $Y_{\text{AC/X}}$ were calculated using the glucose and acetate concentrations at X_{max}

D, F: q_s and q_p were calculated using the μ before induction and the yields obtained at X_{max}

G, I: $Y_{\text{TP/X}}$ and $Y_{\text{RP/X}}$ were calculated using maximum values of protein concentrations

H, J: Percentage of rHuGM-CSF in TP and IBs was based on the densitometric analysis from bands identified in SDS-PAGE gels

Afterward, IBs from *E. coli* cultures growing at 30 or 34 °C with induction at 42 °C were purified by multiple washing steps. The band corresponding to rHuGM-CSF was visible only in the IBs after the upshift to 42 °C, regardless of the growth temperature, but not in the soluble protein fraction (Supplemental Fig. S3). Subsequently, to determine the rHuGM-CSF yields in the insoluble fraction, 20 μg of IBs obtained at different post-induction times (1, 3, 5, 10, and 18/20 h) from *E. coli* cultures that grew at 30 or 34 °C were analyzed on 15% SDS-PAGE (Fig. 2). The European Pharmacopoeia reference standard for human GM-CSF (Molgramostim) was used as a positive control (Molgra St. in Fig. 2). The accumulation of rHuGM-CSF in IBs showed differences depending on the growth (pre-induction) temperature (Fig. 2). Densitometric analysis of the rHuGM-CSF protein in IBs indicated the content of $\sim 45 \pm 2\%$ and $\sim 53 \pm 3\%$ of recombinant protein in thermoinduced cultures, from 5 h to the end of the culture, that grew at 30 and 34 °C, respectively (Table 1). Although the total protein concentration at the end

of cultures was higher in those that follow 30 °C → 42 °C, (Fig. 3A), the amount of protein (Fig. 3B) and rHuGM-CSF within the IBs was higher in those 34 °C → 42 °C (Table 1). The rHuGM-CSF per biomass yield ($Y_{\text{RP/X}}$) was two times higher for cultures of 34 °C → 42 °C (0.12 ± 0.02 g/g) than for those of 30 °C → 42 °C (0.06 ± 0.03 g/g), demonstrating that the bacterial growth at 34 °C favored the accumulation of rHuGM-CSF in IBs during thermoinduction (Table 1).

Main folding chaperones (DnaK and GroEL) are associated with IBs and their co-chaperones (DnaJ and GroES) to the soluble protein fraction during thermoinduction

Here, immunodetection of the main folding chaperones (DnaK and GroEL) and their co-chaperones (DnaJ and GroES) was carried out (Fig. 4). As positive controls, total protein lysates of the recombinant *E. coli* W3110 growing at 30 or 34 °C without thermoinduction and whole protein

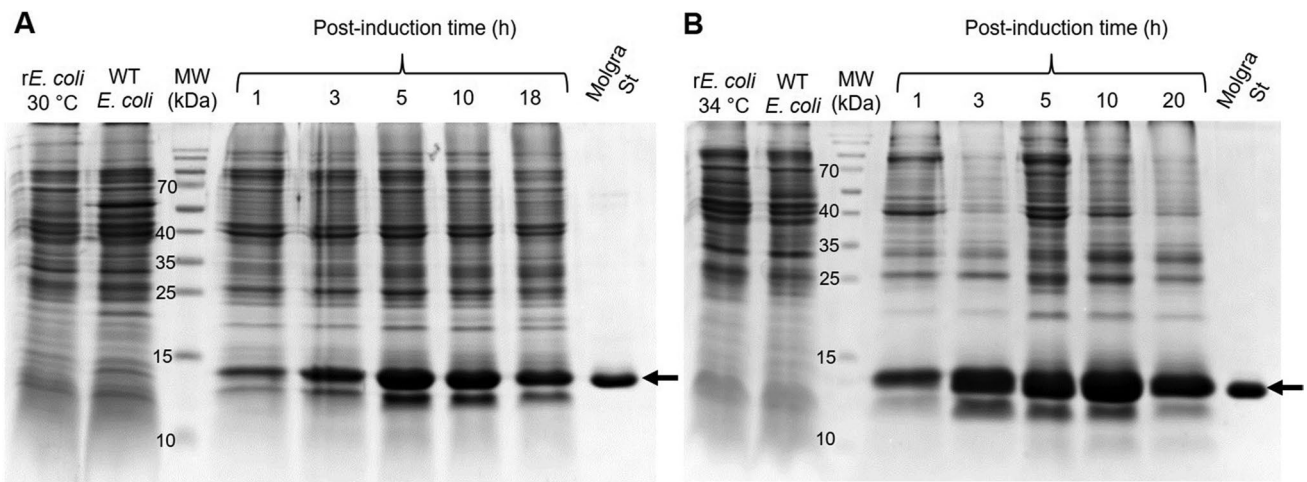
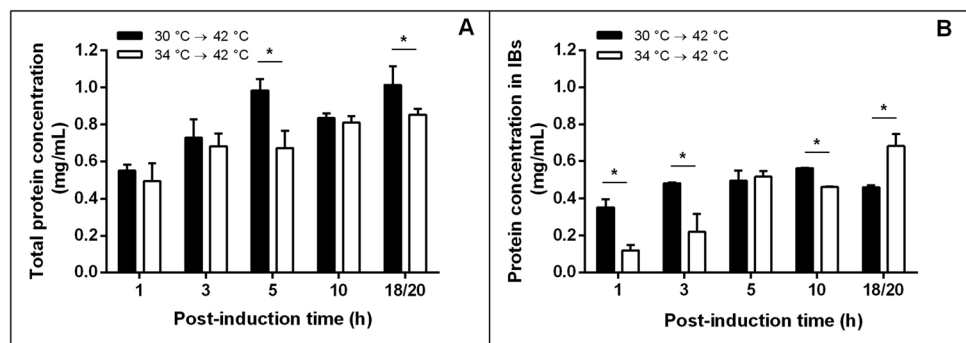


Fig. 2 Analysis of protein in IBs by 15% SDS-PAGE gel stained with Coomassie blue. Purified IBs from *E. coli* W3110 bioreactor cultures growing at 30 °C (A) or 34 °C (B) with subsequent rHuGM-CSF thermoinduction at 42 °C are presented. Lane *rE. coli* 30 °C and lane *rE. coli* 34 °C: total protein of the recombinant *E. coli* W3110 without thermoinduction growing at 30 or 34 °C, respectively; Lane WT

E. coli: total protein from wild-type *E. coli* W3110 strain. Lane MW: molecular weight marker. IBs from different post-induction times (1, 3, 5, 10, and 18/20 h) to the two conditions evaluated are shown. Molgra St: Molgramostim reference standard (2 µg). Arrows indicate the band corresponding to the rHuGM-CSF protein (~ 14 kDa)

Fig. 3 The concentration of total protein (A) and protein in IBs (B) of *E. coli* W3110 cultures under different pre-induction temperatures: 30 °C (black bars) or 34 °C (white bars) and subsequent rHu-GM-CSF thermoinduction at 42 °C. The mean and standard deviation for three biological replicates per condition are shown



lysates from wild-type *E. coli* W3110 were used. In both control fractions, the HSPs mentioned were identified, as expected (Lanes 1 and 2, Fig. 4). DnaK chaperone with an approximate molecular weight of 70 kDa (Bardwell and Craig, 1984) was found weakly expressed 1 and 3 h after thermoinduction, but the intensity of the band increased at 5 h after thermoinduction and returned to a baseline level at the end of cultivation, both in IBs from *E. coli* that grew at 30 °C → 42 °C (Fig. 4A, Panel 1) and 34 °C → 42 °C (Fig. 4B, Panel 1). However, at 34 °C → 42 °C the band for DnaK (Fig. 4B, Panel 1) was noticeably stronger than at 30 °C → 42 °C (Fig. 4A, Panel 1). In the case of the GroEL chaperone, a band close to 60 kDa was observed in the IBs obtained either at a growth temperature of 30 °C (Fig. 4A, Panel 3) or 34 °C (Fig. 4B, Panel 3), being of similar intensity during all time after thermoinduction at 42 °C.

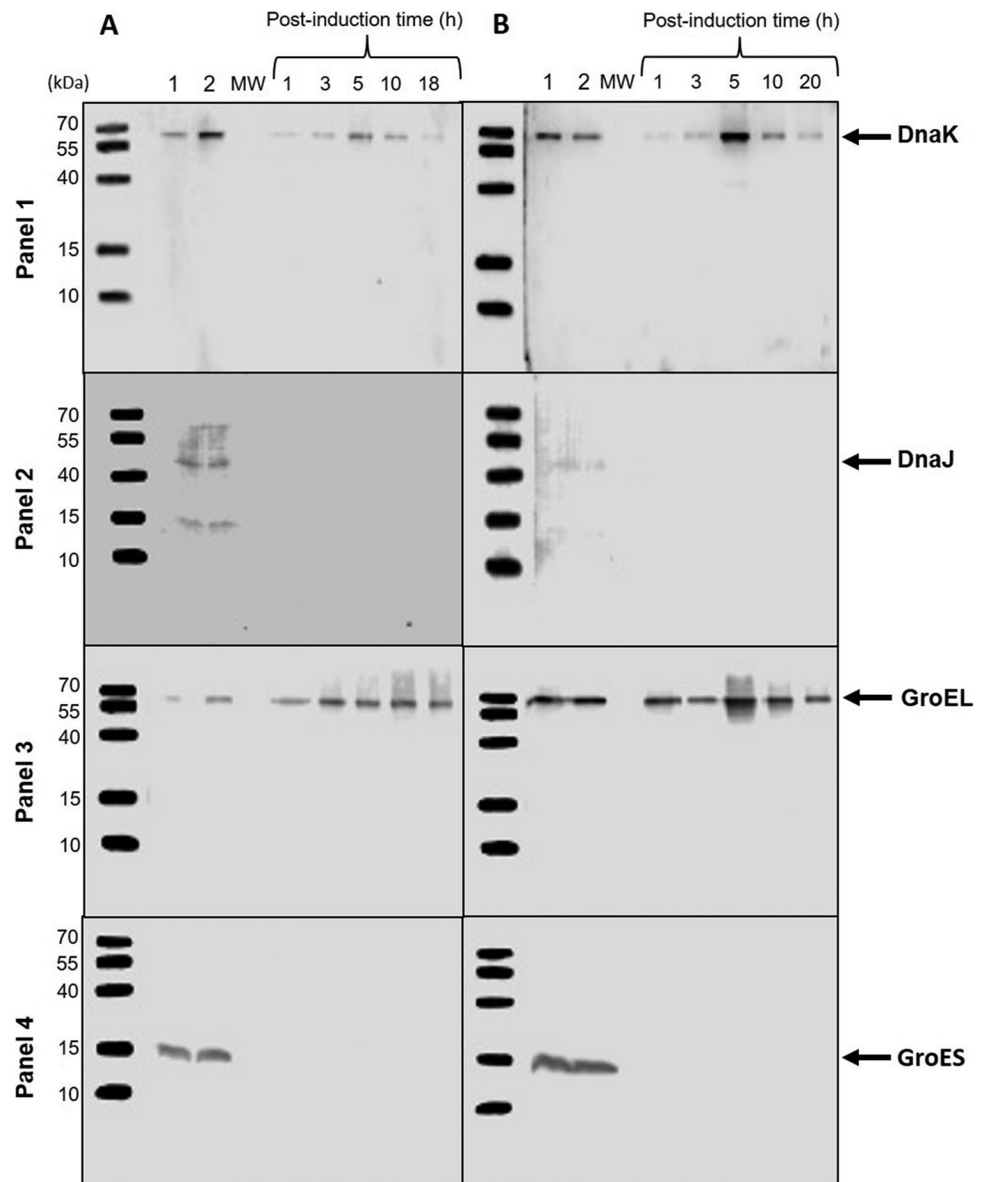
The immunodetection of the co-chaperones DnaJ with ~ 41 kDa (Fig. 4, Panel 2) and GroES with ~ 15 kDa (Fig. 4, Panel 4) was performed, and the bands corresponding

to these two proteins were only observed in lanes 1 and 2, which belong to the positive controls. That is, DnaJ and GroES are not associated with IBs under either of the two pre-induction temperatures tested but remain in the soluble fractions of the non-induced recombinant and the wild-type strains. Finally, GroES and DnaJ co-chaperones were immunodetected in the total soluble protein from *E. coli* cultures growing at 30 °C and 34 °C with thermoinduction at 42 °C (Supplemental Fig. S4).

The pre-induction temperature influenced the content of amyloid-like structure in IBs in a thermoinducible system

The effect of pre-induction temperature (30 or 34 °C) on the amyloid content of rHuGM-CSF IBs obtained under thermoinduction at 42 °C (1 h, 3 h, 5 h, 10 h, and 18/20 h) was analyzed by ATR-FTIR (Fig. 5). ATR-FTIR is a sensitive technique to determine the secondary structure of proteins

Fig. 4 Immunodetection of DnaK, DnaJ, GroEL, and GroES chaperones in rHuGM-CSF IBs from cultures under different pre-induction temperatures: 30 °C (A) or 34 °C (B) and subsequent thermoinduction at 42 °C. Lanes 1A and 1B: total protein lysates of the recombinant *E. coli* W3110 without thermoinduction growing at 30 or 34 °C, respectively. Lanes 2A and 2B: whole protein lysate from wild-type *E. coli* W3110 strain. Lane MW: molecular weight marker. IBs from different post-induction times (1, 3, 5, 10, and 18/20 h) to the two conditions evaluated are shown. Arrows indicate the bands corresponding to DnaK (~70 kDa, panel 1), DnaJ (~41 kDa, panel 2), GroEL (~60 kDa, panel 3), and GroES (~15 kDa, panel 4). The amount of protein in IBs (20 µg) loaded on the SDS-PAGE gels was used as a loading control for western blotting



and studying aggregates formation (Miller et al. 2013). In particular, the absorbance spectra were obtained in the amide I region (1,700–1,500 cm^{-1}), and second derivatives were used to identify the major bands and assign them to the protein secondary structure components (Fig. 5A, B). The major band at 1654 cm^{-1} was assigned as α -helices/random coil, while the bands at 1636 cm^{-1} and 1625 cm^{-1} were designated as β -sheets in native structure (β -sheets) and intermolecular β -structures related to amyloid conformation (aggregates), respectively (Ami et al. 2006; Li et al. 2019; Singh et al. 2020). The rHuGM-CSF IBs from cultures growing at 30 °C \rightarrow 42 °C (Fig. 5A) exhibited a higher spectral intensity of the band at 1625 cm^{-1} compared to IBs from cultures growing at 34 °C \rightarrow 42 °C (Fig. 5B), indicating a decrease in the content of amyloid aggregates when the pre-induction temperature is increased. The content of

α -helices and β -sheets in the IBs did not differ significantly for both pre-induction temperatures. Furthermore, no clear differences were observed between the ATR-FTIR spectra of the IBs concerning the post-induction time (Fig. 5A, B). The minima of the second derivative of each structural component allow to observe the differences between the secondary structure content under the evaluated conditions (Fig. 5C, D, E). From the first hour after thermoinduction, the content of amyloid aggregates was higher for IBs from cultures grown at 30 °C than at 34 °C (Fig. 5E). Moreover, the content of α -helices (Fig. 5C) and β -sheets (Fig. 5D) was similar in rHuGM-CSF IBs, regardless of the pre-induction temperature and post-induction time.

Alternatively, amyloid-diagnostic dyes are used to determine amyloid-like structure in IBs (Carrió et al. 2005; De Groot et al. 2009; Singh et al. 2020). Thioflavin T (Th-T)

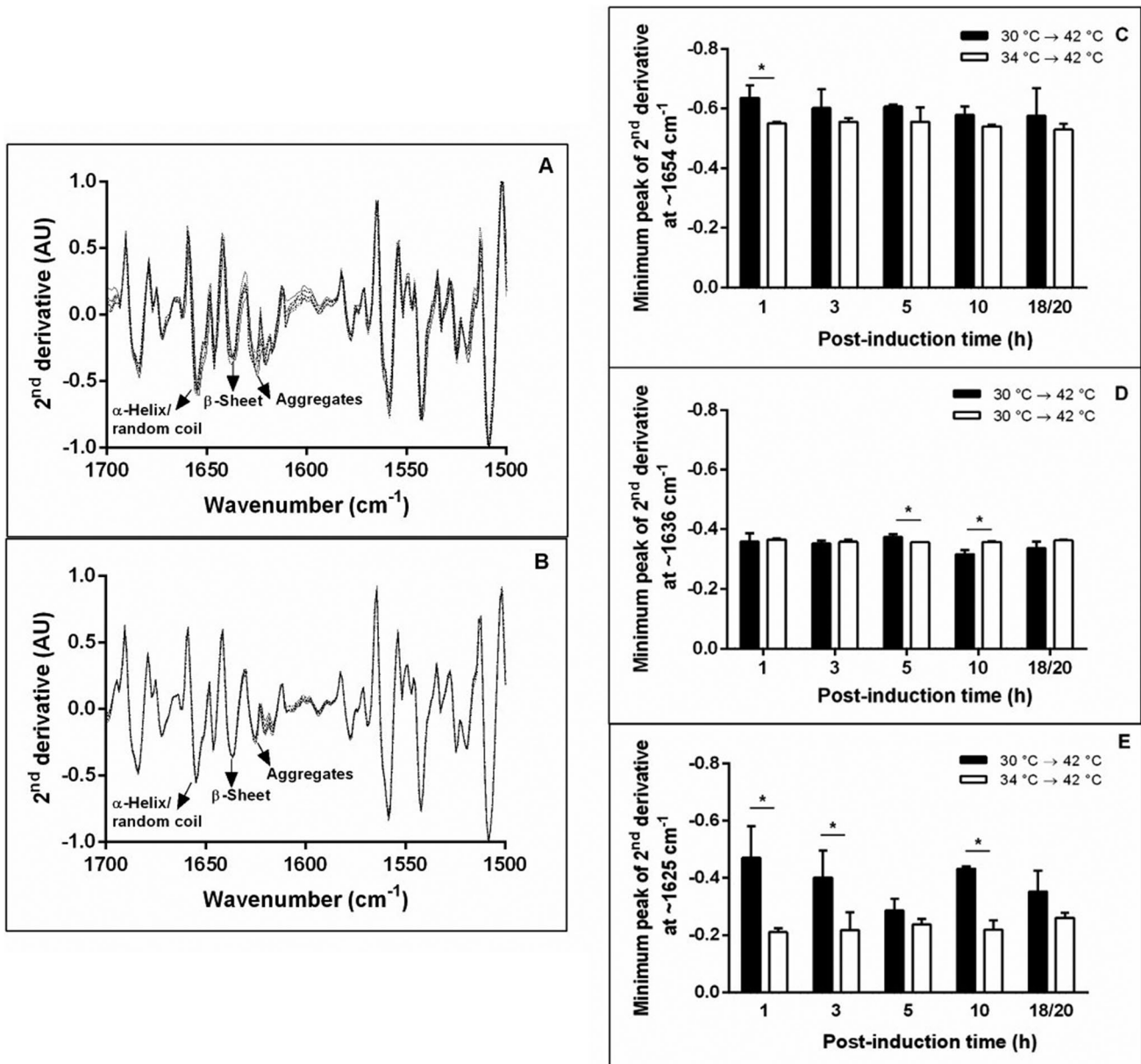


Fig. 5 Amyloid content in rHuGM-CSF IBs by ATR-FTIR. Second derivatives of the absorbance spectra for IBs from cultures growing at 30 °C (A) or 34 °C (B) and harvested at different times after thermoinduction at 42 °C: 1 h (solid line), 3 h (dashed line), 5 h (dotted line), 10 h (dashed-dotted line) and 18/20 h (dashed double-dotted line). Data were normalized with respect to the tyrosine peak (~1508 cm⁻¹), and the major bands were used to identify and assign structural components as α helix/random coil (~1654 cm⁻¹), β sheets

(~1636 cm⁻¹), and amyloid aggregates (~1625 cm⁻¹). Spectra represent the average of three biological replicas. Comparison of the second derivatives minima corresponding to α helix/random coil (C), β sheets (D), and amyloid aggregates (E) of IBs from cultures at 30 °C (black bars) or 34 °C (white bars) collected at different times after thermoinduction at 42 °C. The mean and standard deviation are shown for three independent experiments

is a specific marker to study the amyloid conformation in aggregates since it binds to the surface of channels formed by cross-linked β -sheets (Krebs et al. 2005; Wu et al. 2009). A higher fluorescence indicates a higher amyloid content (LeVine 1995; Castellanos-Mendoza et al. 2014). The change in the fluorescence spectra of Th-T was evaluated after incubation with the rHuGM-CSF IBs (Fig. 6). The

maximum emission fluorescence was around 485 nm, both for IBs from cultures 30 °C → 42 °C and 34 °C → 42 °C, which is a typical feature of amyloid aggregates (Singh et al. 2020). IBs collected from cultures grown at 30 °C → 42 °C showed a gradual increase in fluorescence intensity over time, that is, the amount of amyloid structure was greater at 18 h post-induction (Fig. 6A). In contrast, the fluorescence

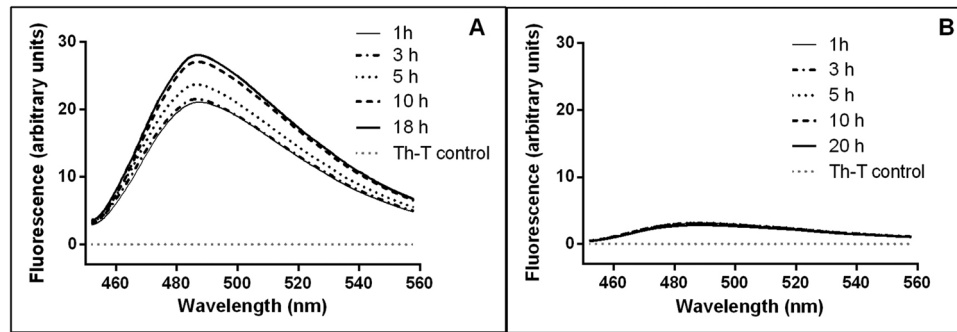


Fig. 6 Fluorescence emission spectra of Th-T binding to rHuGM-CSF IBs obtained under pre-induction temperatures of 30 °C (**A**) or 34 °C (**B**) and thermoinduction at 42 °C. IBs were harvested at different times post-induction: 1 h (thin solid line), 3 h (dashed-dotted

line), 5 h (dotted line), 10 h (dashed line), and 18/20 h (thick solid line). The spectrum of Th-T without protein was used as a control (dotted gray line), and the mean of two biological replicates per condition is shown

signal of Th-T was minimal for the IBs produced in cultures carried out at 34 °C → 42 °C (Fig. 6B), suggesting either a lack of amyloid structures in these aggregates or the inability of binding to them due to greater compaction or a small size (Carrió et al. 2005).

Pre-induction temperature impacts the resistance to proteolytic degradation and solubilization of IBs.

Evaluation of the IBs resistance to proteolytic degradation with proteinase K (PK) has been helpful to characterize the molecular organization and stability of aggregates, as well as an indication of their amyloid content (Castellanos-Mendoza et al. 2014; Calcines-Cruz et al. 2018; Restrepo-Pineda et al. 2019; Singh et al. 2020). PK is a serine protease that exhibits low activity on regions structurally dominated by β -sheets, typical of amyloid fibrils, but it is highly active in hydrophilic domains enriched by loops and α -helices (De Groot et al. 2009; Vázquez-Fernández et al. 2012; Macedo et al. 2015). The enzymatic activity of PK on the IBs was monitored for 100 min at 350 nm (Fig. 7). IBs from *E. coli* cultures of 34 °C → 42 °C were more susceptible to proteolytic attack by PK (Fig. 7B) than IBs from cultures of 30 °C → 42 °C (Fig. 7A). In the first hours after thermoinduction, IBs from 30 °C → 42 °C appeared to be more susceptible to PK digestion than IBs collected during the final hours (Fig. 7A); the same behavior was observed at 34 °C → 42 °C, where IBs obtained at 1, 3 and 5 h post-induction showed less resistance to PK activity than IBs harvested at 10 and 20 h (Fig. 7B). This means that the pre-induction temperature and the post-induction time affect the structural arrangement of the protein aggregates and, at the same time, their resistance to enzymatic digestion.

Solubilization of rHuGM-CSF IBs against increasing concentrations of guanidinium chloride was determined.

GndHCl is a strong chaotropic agent whose ionic nature causes denaturation of globular proteins and provides an estimate of the conformational stability of IBs (Monera et al. 1994; Del Vecchio et al. 2002; Castellanos-Mendoza et al. 2014). In Fig. 8, the solubilization profiles of rHuGM-CSF IBs exhibit a similar trend under the two evaluated pre-induction temperatures (30 and 34 °C). Protein aggregates obtained after thermoinduction were sensitive to chemical solubilization. At 1 M GndHCl, the amount of solubilized protein was small, but it increased at higher concentrations of GndHCl (3 and 5 M) (Fig. 8). Statistical analysis indicated that the concentrations of solubilized protein did not present significant differences with respect to the post-induction time (Fig. 8).

After IBs solubilization in GndHCl (6 M) and folding process, rHuGM-CSF was purified by HPLC showing a retention time of ~24.5 min, in both, 30 °C → 42 °C and 34 °C → 42 °C (Fig. 9). A similar retention time was observed when the European Pharmacopoeia reference standard for human GM-CSF was injected in the HPLC (inset of Fig. 9). All the small peaks observed before and after the rHuGM-CSF peak are surely the host cell proteins from the IBs. Finally, the refolding ability of the solubilized rHuGM-CSF was assayed by CD spectroscopy. In the far-UV region, the asymmetric environments of peptide bonds yield CD signals that are characteristic of each different structural element, allowing the secondary structure of a protein to be estimated. As shown in Fig. 10, protein samples obtained from both thermoinduction regimens showed DC spectra largely overlapping each other, exhibiting two minima centered ~208 and ~220 nm that are typical of helical-type secondary structures. Deconvolution analysis of these spectra yielded α -helix and β -strand contents of 36% and 15%, respectively, which agree with those of the crystallographic structure of the protein, α -helix = 39% and β -strand = 9% (PDB code 1csg; Walter et al. 1992).

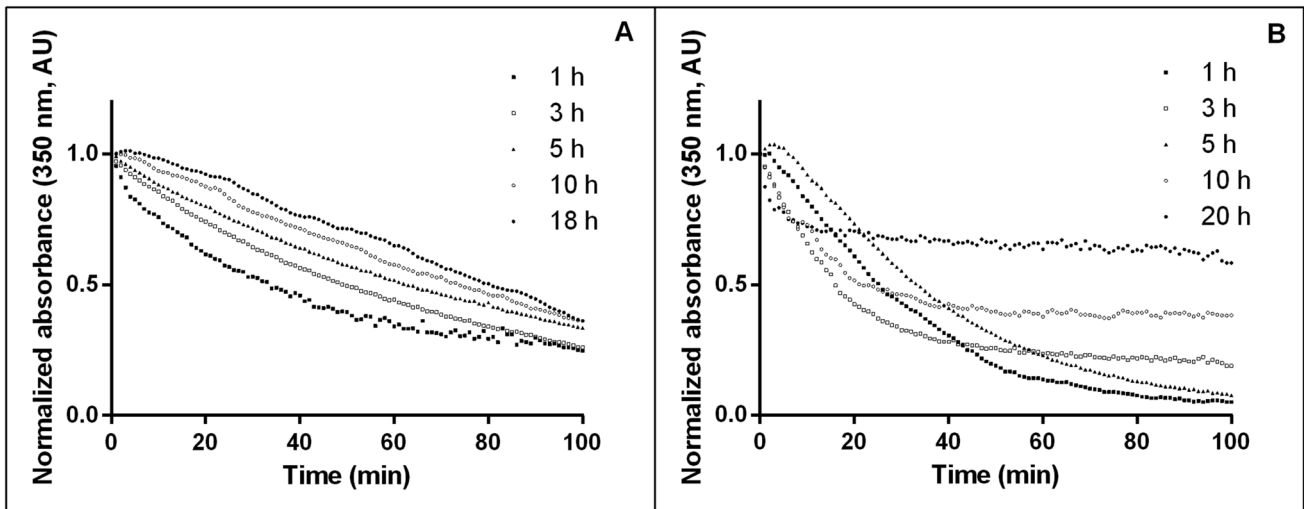


Fig. 7 Kinetics of proteolytic digestion of rHuGM-CSF IBs with proteinase-K from cultures obtained at different pre-induction temperatures: 30 °C (A) or 34 °C (B) and subsequent thermoinduction at 42 °C. IBs were collected at different times post-induction: 1 h (black

circles), 3 h (white circles), 5 h (triangles), 10 h (white squares) and 18/20 h (black squares). The progressive degradation was followed by absorbance at 350 nm for 100 min, and data were normalized. Traces represent the average of at least two independent experiments

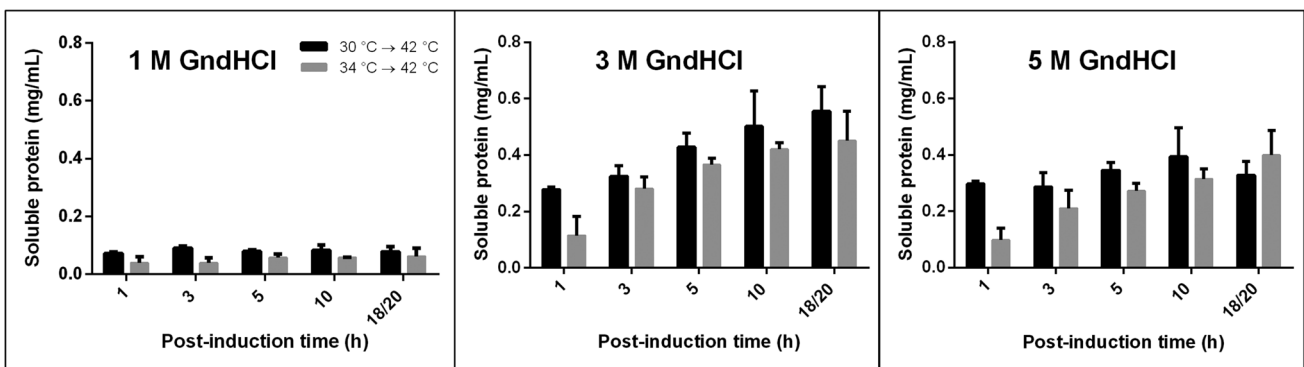


Fig. 8 Solubilization profiles of rHuGM-CSF IBs obtained from pre-induced cultures at 30 °C or 34 °C after different times of thermoinduction at 42 °C (1, 3, 5, 10 and 18/20 h). The amount of solubilized protein (mg/ml) after 24 h of incubation with 1 M (A), 3 M (B), and

5 M (C) concentrations of guanidinium chloride is presented. Bars indicate the mean and standard deviation of the data obtained at each time from three independent experiments

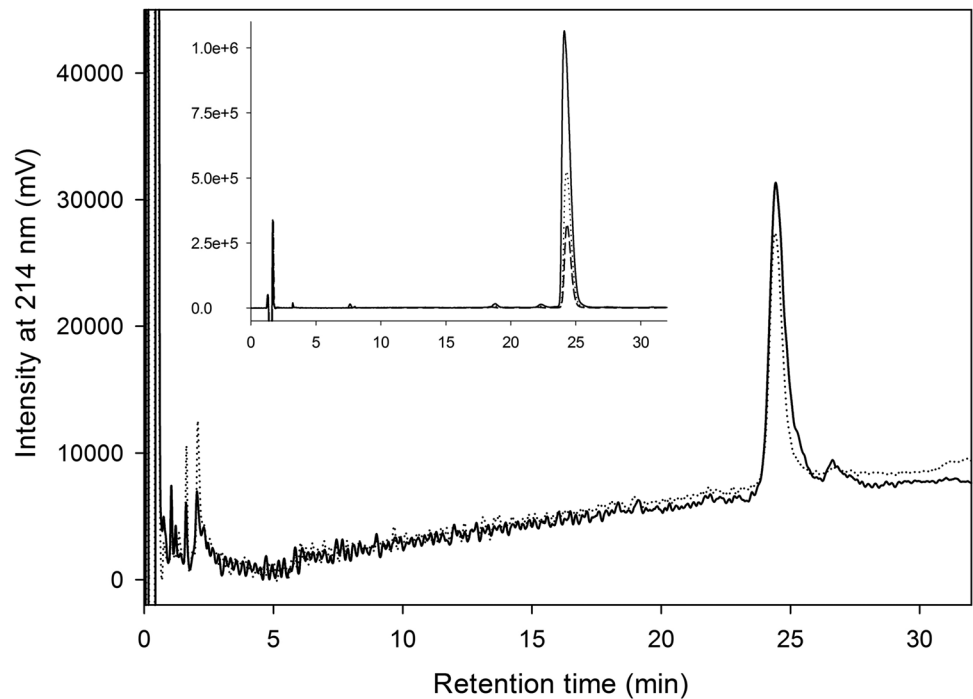
Discussion

Innumerable bioprocesses of recombinant protein production for therapeutic use are carried out in *E. coli*, and the formation of bacterial aggregates has become a common phenomenon that, contrary to being relegated, has gained interest in recent years (García-Fruitós et al. 2010; De Marco et al. 2019; Pesarrodonna et al. 2019; Jäger et al. 2020). Inclusion bodies (IBs) are enriched reservoirs of recombinant protein, which can be considered a previous protein purification step (De Marco et al. 2019; Restrepo-Pineda et al. 2021). In thermoinducible systems, the recombinant protein overexpression, the heat shock response, and IBs formation co-occur in the cells (Valdez-Cruz et al. 2010; Restrepo-Pineda

et al. 2021a). Therefore, understanding the communication between molecular responses and physiological events in this system can be useful to design optimized production bioprocesses that allow higher yields of biologically active recombinant protein with inexpensive and straightforward recovery steps from IBs (Rosano et al. 2019; Restrepo-Pineda et al. 2021).

In thermoinducible systems, the temperature upshifts and the over synthesis of recombinant proteins and HSPs cause an increase in energy demand, metabolic alterations, and a decrease in cell growth (Hoffmann and Rinas 2004; Restrepo-Pineda et al. 2021). Our study shows the effect of pre-induction temperature on cell growth, chaperone composition, and structural characteristics of IBs collected at

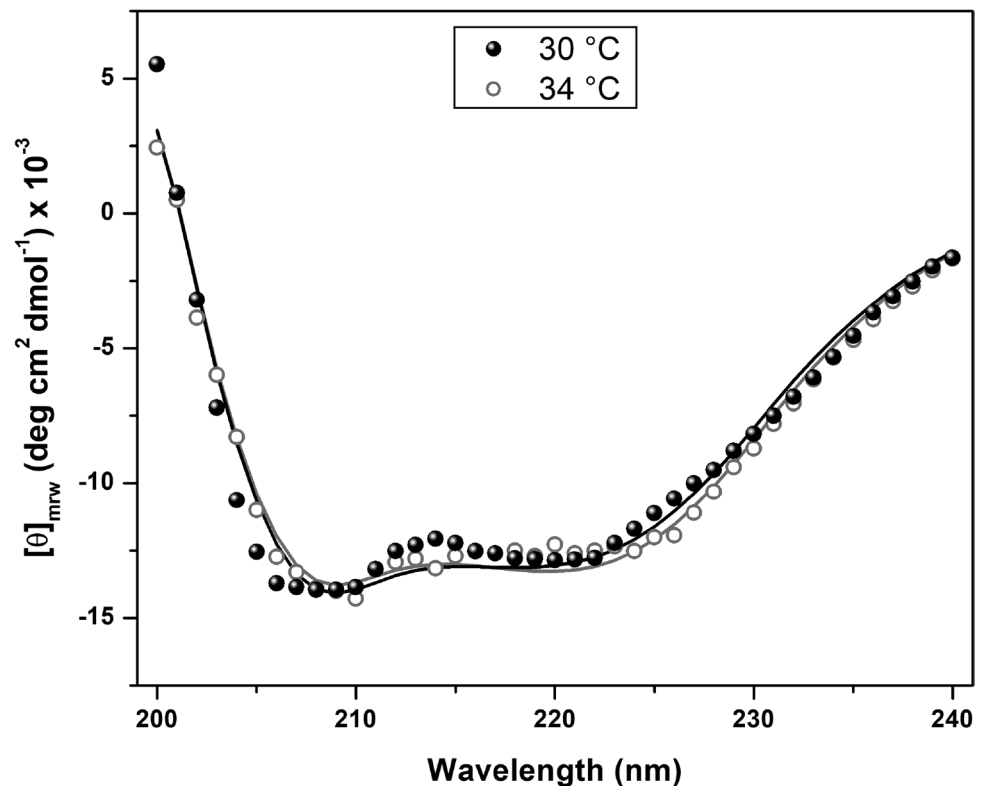
Fig. 9 Purification of the folded rHuGM-CSF by reverse-phase HPLC. The folded protein solution (~ 10 µg) from pre-induced cultures at 30 °C (continuous line) or 34 °C (dotted line) after thermoinduction at 42 °C was loaded in the HPLC at 50 °C with a detector wavelength of 214 nm. A standard curve (inset) of the European Pharmacopoeia reference standard for human GM-CSF (Molgramostim, Y0000251, Sigma Aldrich, St. Louis, MO, USA) was carried out at 1.345, 0.672, and 0.336 mg/ml



different times of thermoinduction from cultures producing the rHuGM-CSF. *E. coli* W3110 growing either at 30 °C or 34 °C reached similar maximum biomass. However, a significant increase in the specific growth rate (μ), the specific glucose consumption rate (q_g), and the specific acetate

formation rate (q_p) was evidenced by increasing the pre-induction temperature (Fig. 1, Table 1). In previous publications, the production of recombinant proteins under the $\lambda pL/pR$ -c1857 thermoinducible system was also accompanied by the acetate accumulation, reporting values near 4.0 g/l in *E.*

Fig. 10 Far-UV circular dichroism spectra of purified rHuGM-CSF in water from IBs obtained from pre-induced cultures at 30 °C (filled circles) or 34 °C (open circles) after thermoinduction at 42 °C. Each spectrum corresponded to the average of three repetitive scans and was corrected by the buffer signal



coli BL21 (Caspeta et al. 2009, 2013); 0.2 g/l in *E. coli* K-12 (Mansey et al. 2014); 3.5–7.4 g/l in *E. coli* 53,606 (Restrepo-Pineda et al. 2019) and 5.9–11.3 g/l in *E. coli* W3110 (this work). Aerobic *E. coli* cultures under conditions of excess glucose (20–40 g/l) are accompanied by metabolic overflow, which can lead to high excretion of acetate and other by-products (Wittmann et al. 2007; Phue and Shiloach 2004). This acetate accumulation is due to a flow redirection from pyruvate dehydrogenase to pyruvate oxidase to remedy the pyruvate node load during induction (Wittmann et al. 2007; Shiloach and Rinas 2009). Concentrations above 2.4 g/l of acetate in the culture medium can generate a decrease in bacterial growth and inhibit recombinant protein production (Dittrich et al. 2005; Eiteman and Altman 2006), which could be associated with the fall in biomass at the end of thermoinduced cultures (Fig. 1) as it can also be due to a complete depletion of the carbon (Restrepo-Pineda et al. 2019).

Bacterial growth at 34 °C favored the accumulation of rHuGM-CSF in IBs during thermoinduction at 42 °C in comparison with a pre-induction of 30 °C, possibly due to those bacterial cells grown at 34 °C have an accelerated rate of cellular processes, reflected in a higher specific growth rate compared to 30 °C. This may be associated with an increased rate of translation, a higher concentration of nascent recombinant polypeptide in the cytosol, and, therefore, the probability of stereo-specific interactions that lead to the increase of rHuGM-CSF aggregation (Singh et al. 2020; Adachi et al. 2015). In addition, it is possible that cells cultivated at 30 °C require more resources to deal with heat stress; while the cells that grew at 34 °C already have a physiological and metabolic pre-adaptation to thermal stress, favoring productivity (Cullum et al. 2001). According to these, the pre-induction temperature is modifying not only the specific growth rate but also the post-induction recombinant protein synthesis rate and its accumulation in IBs. The cellular growth rate has been related to the IBs amount, and biological activity of the recombinant protein produced in them. Iafolla et al. (2008) found that at the fastest growth rate, more active EGFP (enhanced green fluorescent protein) was present in IBs, while at slower growth rate IBs are less abundant and with less active EGFP (Iafolla et al. 2008).

The tendency of GM-CSF to aggregation makes it an ideal candidate protein to study the behavior at the structural and compositional level of IBs obtained from thermoinduced cultures. The first studies about the GM-CSF production in bacteria were based on a temperature-inducible plasmid (from 28 to 42–48 °C). They reported that both murine GM-CSF (DeLamarter et al. 1985) and human GM-CSF (Burgess et al. 1987) accumulated in IBs when produced in *E. coli*, which agrees with our results. This knowledge has been corroborated in subsequent reports using chemical induction with IPTG (Schwanke

et al. 2009; Thomson et al. 2012) or autoinduction (Malekian et al. 2019a). However, those did not analyze the protein secondary structure or the amyloid content of the aggregates, they only demonstrated the bioactivity of the recombinant GM-CSF obtained from IBs. The human GM-CSF produced in *E. coli* under the regulation of a heat-inducible promoter showed a specific activity of 2.9×10^7 units/mg with bone marrow cells (Burgess et al. 1987). Recombinant Murine-derived GM-CSF stimulated the growth of granulocyte and macrophage colonies of mouse bone marrow cells (DeLamarter et al. 1985). The refolded and purified rHuGM-CSF promoted the cell growth in a human hematopoietic cell line in a similar way to the commercially available protein (Schwanke et al. 2009; Thomson et al. 2012). Notably, these results indicate that the recombinant protein reaches an active conformation after recuperation and refolding from IBs and, confirms that the absence of glycosylation or the addition of an extra N-terminal methionine residue does not affect the bioactivity of the rHuGM-CSF obtained on a bacterial platform (Burgess et al. 1987; DeLamarter et al. 1985).

E. coli has robust control systems to assist the folding of newly synthesized proteins in the cytosol, including the DnaK chaperone with its DnaJ and GrpE co-chaperones, and GroEL chaperone with its GroES co-chaperone (Houry 2001; Bhandari and Houry 2015). In this work, molecular chaperones were differentially associated with the protein fractions, detecting DnaK and GroEL in the IBs. At the same time, DnaJ and GroES were found in the total soluble protein, possibly reflecting the order in which they interact with the protein folding intermediates during aggregation. Differences in DnaK expression due to pre-induction temperature suggest that DnaK is preferentially required at elevated temperatures to maintain viable cell growth and other multiple bacterial functions (Mayer 2021). Previous results indicate that *E. coli* cells with *dnak* null mutations can grow slowly at 30 °C and 37 °C, but at 42 °C they lose the ability to form colonies after 2 h of exposure (Paek and Walker 1987). In contrast, the constant production of GroEL throughout the thermoinduction stage and under the two growth temperature conditions evaluated corroborates its importance as a central regulator for protein folding in *E. coli* (Hayer-Hartl et al. 2015). Some studies have reported that GroEL complies a job of protecting the bacterial growth in a wide range of temperatures, from low (17 to 30 °C; Fayet et al. 1989) to normal/high temperatures (20 to 40 °C; Kusakawa and Yura 1988). In brief, GroEL seems to act as a key piece in supporting growth at normal physiological temperatures, whereas DnaK might be essential mostly at higher temperature. Some studies have revealed the presence of chaperones such as DnaK, GrpE, GroEL, GroES, IbpA and IbpB in IBs isolated from *E. coli* after induction by IPTG or temperature increase, but they did not find DnaJ (Hoffmann and Rinas

2000; Rinas et al. 2007; Jürgen et al. 2010). The absence of DnaJ was not discussed in those reports, probably because it is assumed that it remains in the soluble fraction like most HSPs (> 90%; Hoffmann and Rinas 2000).

In recent years, it has been proposed that the structural properties of IBs define the protocols of isolation, solubilization, and refolding, mainly during recovery of a biologically active recombinant protein (Singh and Panda 2005; Singhvi et al. 2020). Structural changes of IBs depend not only on the dynamic of aggregation and nature of the recombinant protein but also on the bioprocess conditions (Castellanos-Mendoza et al. 2014; Calcines-Cruz et al. 2018; Restrepo-Pineda et al. 2019; De Marco et al. 2019). Structural analyses by ATR-FTIR and binding to Th-T indicated that at a higher pre-induction temperature (34 °C), the IBs have a lower proportion of amyloid-like conformations than at 30 °C (Figs. 5 and 6). Moreover, previous studies revealed that regions with higher amyloid-like conformation in IBs are more resistant to proteolysis with by PK (Upadhyay et al. 2012). Therefore, the degradation profiles in Fig. 7 also confirm the results observed in the secondary structure analysis by ATR-FTIR and binding to Th-T, suggesting that the rHuGM-CSF IBs obtained at 30 °C → 42 °C have a higher proportion of amyloid-like structure compared to IBs obtained at 34 °C → 42 °C.

Usually, high concentrations of urea or GndHCl (6–8 M) are used in the solubilization of IBs, which can cause a significant disturbance in the structure of the recombinant protein folded state and result in a low recovery of bioactive protein (Upadhyay et al. 2012, 2016; Singhvi et al. 2020). In this study, the rHuGM-CSF IBs were effectively solubilized in low concentrations of GndHCl (3 M and 5 M, Fig. 8), which is important in the downstream process at the industrial level. When IBs can be solubilized at the lowest possible denaturant concentration, it can result in proteins that retain part of their folded structure, making refolding processes more efficient and consequently recovering biological activity (Singh et al. 2015). Indeed, the removal of the denaturing agent yielded folded proteins with native-like secondary structure contents, as revealed by the HPLC purification recovering the folded rHuGM-CSF (Fig. 9), as also by solution CD spectroscopy (Fig. 10). CD is a widely used tool to identify changes in the secondary structure of proteins, which can impact their mechanism of action or in the regulation of their biological activity (Kelly and Price 2000; Kelly et al. 2005). The application of CD to analyze the protein structure after denaturalization, and to associate these data with the rate of recovery of biological activity is common (Kelly and Price 1997). In this study, CD spectra of rHuGM-CSF from *E. coli* cultures growing either at 30 or 34 °C were similar (Fig. 10) A typical helical conformation with two negative shoulders at ~208 and ~220 nm was observed. Calculations of the secondary structure suggest 36% α -helix and

15% β -strand for both conditions, which agrees with previously reported values of ~30% α -helix content for recombinant GM-CSF by far-UV CD (Malekian et al. 2019b; Wingfield et al. 1988). The refolded rHuGM-CSF characterization by CD allowed obtaining valuable insights to understand the protein structure–function relationship.

The claims obtained in this study could serve as a methodological proposal to produce biopharmaceutical proteins in IBs using thermoinduced systems. By modifying the growth or pre-induction temperature, it is possible to have conformationally different IBs with a high content of recombinant protein, and easier to solubilize, lowering bioprocesses efforts and costs. Moreover, the similarity in the secondary structure content between the recombinant protein isolated from bacterial aggregates and the reported structure of rHuGM-CSF revealed the possibility of obtaining biologically active protein after solubilization and refolding processes.

Supplementary Information The online version contains supplementary material available at <https://doi.org/10.1007/s00253-022-11908-z>.

Acknowledgements Sara Restrepo-Pineda is a doctoral student from “Programa de Doctorado en Ciencias Biológicas” of the “Universidad Nacional Autónoma de México” (UNAM) and received fellowship from CONACYT (CVU 589949), authors thank both institutions for the support provided. EG-H, NS-P, NOP, MAT-R and NAV-C are members of the Sistema Nacional de Investigadores, Consejo Nacional de Ciencia y Tecnología. This project was developed under the Institutional Program of the Instituto de Investigaciones Biomédicas UNAM: “La producción de biomoléculas de interés biomédico en bacterias y hongos”. Authors also appreciate the technical support by Dr. Axel Luviano in CD experiments and Diego Rosiles-Becerril and M. Sc. Luis Pablo Ávila-Barrientos in protein refolding and HPLC development.

Author contributions SR-P, NAV-C, EG-H, NS-P contributed to experimentation; SR-P, EG-H, NAV-C, and MAT-R helped in conceptualization; MAT-R and NAV-C contributed to funding acquisition; MAT-R and NAV-C contributed to project administration; MAT-R, NOP, NS-P, EG-H, and NAV-C helped in resources; SR-P, MAT-R, and NAV-C contributed to writing—original draft; SR-P, NOP, NS-P, MAT-R, and NAV-C helped in writing—review and editing.

Funding This work was supported by “Programa de Apoyo a Proyectos de Investigación e Innovación Tecnológica, Universidad Nacional Autónoma de México” (PAPIIT-UNAM IN210822: NAVC, IN211422, IV201220: MATR). The funders had no role in data collection and analysis, decision to publish, or preparation of the manuscript.

Data availability The authors confirm that all relevant data are included in this article and its supplementary information files.

Declarations

Ethics approval This article does not report any studies with human participants or animals performed by the authors.

Conflict of interest NOP works in Probiomed S.A. de C.V., which manufactures recombinant human therapeutic proteins.

References

- Adachi M, So M, Sakurai K, Kardos J, Goto Y (2015) Supersaturation-limited and unlimited phase transitions compete to produce the pathway complexity in amyloid fibrillation. *J Biol Chem* 290(29):18134–18145. <https://doi.org/10.1074/jbc.M115.648139>
- Ami D, Natalello A, Gatti-Lafranconi P, Lotti M, Doglia SM (2005) Kinetics of inclusion body formation studied in intact cells by FT-IR spectroscopy. *FEBS Lett* 579(16):3433–3436. <https://doi.org/10.1016/j.febslet.2005.04.085>
- Ami D, Natalello A, Taylor G, Tonon G, Doglia SM (2006) Structural analysis of protein inclusion bodies by Fourier transform infrared microspectroscopy. *Biochim Biophys Acta* 1764(4):793–799. <https://doi.org/10.1016/j.bbapap.2005.12.005>
- Assenberg R, Wan PT, Geisse S, Mayr LM (2013) Advances in recombinant protein expression for use in pharmaceutical research. *Curr Opin Struct Biol* 23(3):393–402. <https://doi.org/10.1016/j.sbi.2013.03.008>
- Baeshen MN, Al-Hejin AM, Bora RS, Ahmed MM, Ramadan HA, Saini KS, Redwan EM (2015) Production of biopharmaceuticals in *E. coli*: current scenario and future perspectives. *J Microbiol Biotechnol* 25(7):953–962. <https://doi.org/10.4014/jmb.1412.12079>
- Balchin D, Hayer-Hartl M, Hartl FU (2016) *In vivo* aspects of protein folding and quality control. *Science* 353(6294):aac4354. <https://doi.org/10.1126/science.aac4354>
- Baneyx F, Mujacic M (2004) Recombinant protein folding and misfolding in *Escherichia coli*. *Nat Biotechnol* 22:1399–1408. <https://doi.org/10.1038/nbt1029>
- Bardwell JC, Craig EA (1984) Major heat shock gene of *Drosophila* and the *Escherichia coli* heat-inducible *dnaK* gene are homologous. *Proc Natl Acad Sci USA* 81(3):848–852. <https://doi.org/10.1073/pnas.81.3.848>
- Belew M, Zhou Y, Wang S, Nyström LE, Janson JC (1994) Purification of recombinant human granulocyte-macrophage colony-stimulating factor from the inclusion bodies produced by transformed *Escherichia coli* cells. *J Chromatogr A* 679(1):67–83. [https://doi.org/10.1016/0021-9673\(94\)80312-9](https://doi.org/10.1016/0021-9673(94)80312-9)
- Bhandari V, Houry WA (2015) Substrate interaction networks of the *Escherichia coli* chaperones: trigger factor, DnaK and GroEL. *Adv Exp Med Biol* 883:271–294. https://doi.org/10.1007/978-3-319-23603-2_15
- Bonaventura A, Vecchié A, Wang TS, Lee E, Cremer PC, Carey B, Rajendram P, Hudock KM, Korbee L, Van Tassell BW, Dagna L, Abbate A (2020) Targeting GM-CSF in COVID-19 pneumonia: rationale and strategies. *Front Immunol* 11:1625. <https://doi.org/10.3389/fimmu.2020.01625>
- Burgess AW, Begley CG, Johnson GR, Lopez AF, Williamson DJ, Mermod JJ, Simpson RJ, Schmitz A, DeLamararter JF (1987) Purification and properties of bacterially synthesized human granulocyte-macrophage colony stimulating factor. *Blood* 69(1):43–51. <https://doi.org/10.1182/blood.V69.1.43.43>
- Calcines-Cruz C, Olvera A, Castro-Acosta RM, Zavala G, Alagón A, Trujillo-Roldán MA, Valdez-Cruz NA (2018) Recombinant-phospholipase A2 production and architecture of inclusion bodies are affected by pH in *Escherichia coli*. *Int J Biol Macromol* 108:826–836. <https://doi.org/10.1016/j.ijbiomac.2017.10.178>
- Cano-Garrido O, Rodríguez-Carmona E, Díez-Gil C, Vázquez E, Elizondo E, Cubarsi R, Seras-Franzoso J, Corchero JL, Rinas U, Ratera I, Ventosa N, Veciana J, Villaverde A, García-Fruitós E (2013) Supramolecular organization of protein-releasing functional amyloids solved in bacterial inclusion bodies. *Acta Biomater* 9:6134–6142. <https://doi.org/10.1016/j.actbio.2012.11.033>
- Carrió M, Villaverde A (2003) Role of molecular chaperones in inclusion body formation. *FEBS Lett* 537(1–3):215–221. [https://doi.org/10.1016/S0014-5793\(03\)00126-1](https://doi.org/10.1016/S0014-5793(03)00126-1)
- Carrió M, González-Montalbán N, Vera A, Villaverde A, Ventura S (2005) Amyloid-like properties of bacterial inclusion bodies. *J Mol Biol* 347(5):1025–1037. <https://doi.org/10.1016/j.jmb.2005.02.030>
- Caspeta L, Flores N, Pérez NO, Bolívar F, Ramírez OT (2009) The effect of heating rate on *Escherichia coli* metabolism, physiological stress, transcriptional response, and production of temperature-induced recombinant protein: a scale-down study. *Biotechnol Bioeng* 102(2):468–482. <https://doi.org/10.1002/bit.22084>
- Caspeta L, Lara AR, Pérez NO, Flores N, Bolívar F, Ramírez OT (2013) Enhancing thermo-induced recombinant protein production in *Escherichia coli* by temperature oscillations and post-induction nutrient feeding strategies. *J Biotechnol* 167(1):47–55. <https://doi.org/10.1016/j.jbiotec.2013.06.001>
- Castellanos-Mendoza A, Castro-Acosta RM, Olvera A, Zavala G, Mendoza-Vera M, García-Hernández E, Alagón A, Trujillo-Roldán MA, Valdez-Cruz NA (2014) Influence of pH control in the formation of inclusion bodies during production of recombinant sphingomyelinase-D in *Escherichia coli*. *Microb Cell Fact* 13:1–14. <https://doi.org/10.1186/s12934-014-0137-9>
- Caulcott CA, Rhodes M (1986) Temperature-induced synthesis of recombinant proteins. *Trends Biotechnol* 4:142–146. [https://doi.org/10.1016/0167-7799\(86\)90164-2](https://doi.org/10.1016/0167-7799(86)90164-2)
- Cullum AJ, Bennett AF, Lenski RE (2001) Evolutionary adaptation to temperature. IX. Preadaptation to novel stressful environments of *Escherichia coli* adapted to high temperature. *Evolution* 55(11):2194–2202. <https://doi.org/10.1111/j.0014-3820.2001.tb00735.x>
- Cumming DA (1991) Glycosylation of recombinant protein therapeutics: control and functional implications. *Glycobiology* 1(2):115–130. <https://doi.org/10.1093/glycob/1.2.115>
- Das KM, Banerjee S, Shekhar N, Damodaran K, Nair R, Somani S, Raiker VP, Jain S, Padmanabhan S (2011) Cloning, soluble expression and purification of high yield recombinant hGMCSF in *Escherichia coli*. *Int J Mol Sci* 12(3):2064–2076. <https://doi.org/10.3390/ijms12032064>
- De Groot NS, Ventura S (2006) Effect of temperature on protein quality in bacterial inclusion bodies. *FEBS Lett* 580(27):6471–6476. <https://doi.org/10.1016/j.febslet.2006.10.071>
- De Groot NS, Sabate R, Ventura S (2009) Amyloids in bacterial inclusion bodies. *Trends Biochem Sci* 34(8):408–416. <https://doi.org/10.1016/j.tibs.2009.03.009>
- De Marco A, Ferrer-Mirallas N, Garcia-Fruitós E, Mitraki A, Peternel S, Rinas U, Trujillo-Roldán MA, Valdez-Cruz NA, Vázquez E, Villaverde A (2019) Bacterial inclusion bodies are industrially exploitable amyloids. *FEMS Microbiol Rev* 43:53–72. <https://doi.org/10.1093/femsre/fuy038>
- Del Vecchio P, Graziano G, Granata V, Barone G, Mandrich L, Rossi M, Manco G (2002) Denaturing action of urea and guanidine hydrochloride towards two thermophilic esterases. *Biochem J* 367(3):857–863. <https://doi.org/10.1042/BJ20020695>
- DeLamararter JF, Mermod JJ, Liang CM, Eliason JF, Thatcher DR (1985) Recombinant murine GM-CSF from *E. coli* has biological activity and is neutralized by a specific antiserum. *EMBO J* 4(10):2575–2581. <https://doi.org/10.1002/j.1460-2075.1985.tb03973.x>
- Dittrich CR, Bennett GN, San KY (2005) Characterization of the acetate-producing pathways in *Escherichia coli*. *Biotechnol Prog* 21(4):1062–1067. <https://doi.org/10.1021/bp050073s>
- Dodd IB, Shearwin KE, Perkins AJ, Burr T, Hochschild A, Egan JB (2004) Cooperativity in long-range gene regulation by the lambda CI repressor. *Genes Dev* 18(3):344–354. <https://doi.org/10.1101/gad.1167904>

- Dougan M, Dranoff G, Dougan SK (2019) GM-CSF, IL-3, and IL-5 family of cytokines: regulators of inflammation. *Immunity* 50(4):796–811. <https://doi.org/10.1016/j.immuni.2019.03.022>
- Eiteman MA, Altman E (2006) Overcoming acetate in *Escherichia coli* recombinant protein fermentations. *Trends Biotechnol* 24(11):530–536. <https://doi.org/10.1016/j.tibtech.2006.09.001>
- Espargaró A, Sabate R, Ventura S (2008) Kinetic and thermodynamic stability of bacterial intracellular aggregates. *FEBS Lett* 582:3669–3673. <https://doi.org/10.1016/j.febslet.2008.09.049>
- Fahnert B, Lilie H, Neubauer P (2004) Inclusion bodies: formation and utilization. In: Scheper T (ed) *Physiological stress responses in bioprocesses*. *Adv Biochem Eng* 89:93–142
- Fayet O, Ziegelhoffer T, Georgopoulos C (1989) The *groES* and *groEL* heat shock gene products of *Escherichia coli* are essential for bacterial growth at all temperatures. *J Bacteriol* 171(3):1379–1385. <https://doi.org/10.1128/jb.171.3.1379-1385.1989>
- Francisco-Cruz A, Aguilar-Santelises M, Ramos-Espinosa O, Mata-Espinosa D, Marquina-Castillo B, Barrios-Payan J, Hernandez-Pando R (2014) Granulocyte–macrophage colony-stimulating factor: not just another haematopoietic growth factor. *Med Oncol* 31(1):774. <https://doi.org/10.1007/s12032-013-0774-6>
- García-Fruitós E, Seras-Franzoso J, Vazquez E, Villaverde A (2010) Tunable geometry of bacterial inclusion bodies as substrate materials for tissue engineering. *Nanotechnol* 21(20):205101. <https://doi.org/10.1088/0957-4484/21/20/205101>
- Gil-García M, Navarro S, Ventura S (2020) Coiled-coil inspired functional inclusion bodies. *Microb Cell Fact* 19:117. <https://doi.org/10.1186/s12934-020-01375-4>
- Gill RT, Valdes JJ, Bentley WE (2000) A comparative study of global stress gene regulation in response to overexpression of recombinant proteins in *Escherichia coli*. *Metab Eng* 2(3):178–189. <https://doi.org/10.1006/mben.2000.0148>
- González-Montalbán N, García-Fruitós E, Villaverde A (2007) Recombinant protein solubility—does more mean better? *Nat Biotechnol* 25(7):718. <https://doi.org/10.1038/nbt0707-718>
- Guisbert E, Herman C, Lu CZ, Gross CA (2004) A chaperone network controls the heat shock response in *E. coli*. *Genes Dev* 18(22):2812–2821. <https://doi.org/10.1101/gad.1219204>
- Guisbert E, Yura T, Rhodius VA, Gross CA (2008) Convergence of molecular, modeling, and systems approaches for an understanding of the *Escherichia coli* heat shock response. *Microbiol Mol Biol Rev* 72(3):545–554. <https://doi.org/10.1128/MMBR.00007-08>
- Hamilton JA (2019) GM-CSF-dependent inflammatory pathways. *Front Immunol* 10:2055. <https://doi.org/10.3389/fimmu.2019.02055>
- Hamilton JA (2020) GM-CSF in inflammation. *J Exp Med* 217(1). <https://doi.org/10.1084/jem.20190945>
- Hartl FU, Hayer-Hartl M (2009) Converging concepts of protein folding *in vitro* and *in vivo*. *Nat Struct Mol Biol* 16:574. <https://doi.org/10.1038/nsmb.1591>
- Hayer-Hartl M, Bracher A, Hartl FU (2015) The GroEL–GroES chaperonin machine: a nano-cage for protein folding. *Trends Biochem Sci* 41(1):62–76. <https://doi.org/10.1016/j.tibs.2015.07.009>
- Hengge-Aronis R (1993) Survival of hunger and stress: the role of rpoS in early stationary phase gene regulation in *E. coli*. *Cell* 72(2):165–168. [https://doi.org/10.1016/0092-8674\(93\)90655-a](https://doi.org/10.1016/0092-8674(93)90655-a)
- Hoffmann F, Rinas U (2000) Kinetics of heat-shock response and inclusion body formation during temperature-induced production of basic fibroblast growth factor in high-cell density cultures of recombinant *Escherichia coli*. *Biotechnol Prog* 16(6):1000–1007. <https://doi.org/10.1021/bp0000959>
- Hoffmann F, Rinas U (2004) Stress induced by recombinant protein production in *Escherichia coli*. In: Scheper T (ed) *Physiological stress responses in bioprocesses*. *Adv Biochem Eng* 89:73–92. <https://doi.org/10.1007/b93994>
- Hoffmann F, Weber J, Rinas U (2002) Metabolic adaptation of *Escherichia coli* during temperature-induced recombinant protein production: 1. Readjustment of metabolic enzyme synthesis. *Biotechnol Bioeng* 80:313–319. <https://doi.org/10.1002/bit.10379>
- Houry WA (2001) Chaperone-assisted protein folding in the cell cytoplasm. *Curr Protein Pept Sci* 2(3):227–244. <https://doi.org/10.2174/1389203013381134>
- Huang CJ, Lin H, Yang X (2012) Industrial production of recombinant therapeutics in *Escherichia coli* and its recent advancements. *J Ind Microbiol Biotechnol* 39(3):383–399. <https://doi.org/10.1007/s10295-011-1082-9>
- Iafolla MAJ, Mazumder M, Sardana V, Velauthapillai T, Pannu K, McMillen DR (2008) Dark proteins: effect of inclusion body formation on quantification of protein expression. *Proteins* 72:1233–1242. <https://doi.org/10.1002/prot.22024>
- Jäger VD, Lamm R, Küsters K, Ölçücü G, Oldiges M, Jaeger KE, Büchs J, Krauss U (2020) Catalytically-active inclusion bodies for biotechnology—general concepts, optimization, and application. *Appl Microbiol Biotechnol* 104:7313–7329. <https://doi.org/10.1007/s00253-020-10760-3>
- Jürgen B, Breitenstein A, Urlacher V, Büttner K, Lin H, Hecker M, Schweder T, Neubauer P (2010) Quality control of inclusion bodies in *Escherichia coli*. *Microb Cell Fact* 9:41. <https://doi.org/10.1186/1475-2859-9-41>
- Kaufman HL, Ruby CE, Hughes T, Slingluff CL (2014) Current status of granulocyte–macrophage colony-stimulating factor in the immunotherapy of melanoma. *J Immunother Cancer* 2(1):1–13. <https://doi.org/10.1186/2051-1426-2-11>
- Kaur J, Kumar A, Kaur J (2018) Strategies for optimization of heterologous protein expression in *E. coli*: Roadblocks and reinforcements. *Int J Biol Macromol* 106:803–822. <https://doi.org/10.1016/j.ijbiomac.2017.08.080>
- Kelly SM, Price NC (1997) The application of circular dichroism to studies of protein folding and unfolding. *Biochim Biophys Acta* 1338(2):161–185. [https://doi.org/10.1016/s0167-4838\(96\)00190-2](https://doi.org/10.1016/s0167-4838(96)00190-2)
- Kelly SM, Price NC (2000) The use of circular dichroism in the investigation of protein structure and function. *Curr Protein Pept Sci* 1(4):349–384. <https://doi.org/10.2174/1389203003381315>
- Kelly SM, Thomas JJ, Price NC (2005) How to study proteins by circular dichroism. *BBA-Proteins Proteom* 1751(2):119–139. <https://doi.org/10.1016/j.bbapap.2005.06.005>
- Krebs MR, Bromley EH, Donald AM (2005) The binding of thioflavin-T to amyloid fibrils: localisation and implications. *J Struct Biol* 149(1):30–37. <https://doi.org/10.1016/j.jsb.2004.08.002>
- Kumar J, Chauhan A, Shah RL, Gupta JA, Rathore AS (2020) Amino acid supplementation for enhancing recombinant protein production in *E. coli*. *Biotechnol Bioeng* 117(8):2420–2433. <https://doi.org/10.1002/bit.27371>
- Kusukawa N, Yura T (1988) Heat shock protein GroE of *Escherichia coli*: key protective roles against thermal stress. *Genes Dev* 2(7):874–882. <https://doi.org/10.1101/gad.2.7.874>
- Lang FM, Lee KMC, Teijaro JR, Becher B, Hamilton JA (2020) GM-CSF-based treatments in COVID-19: reconciling opposing therapeutic approaches. *Nat Rev Immunol* 20:507–514. <https://doi.org/10.1038/s41577-020-0357-7>
- LeVine H (1995) Thioflavine T interaction with amyloid β -sheet structures. *Amyloid* 2(1):1–6. <https://doi.org/10.3109/13506129509031881>
- Lewis DEA, Gussin GN, Adhya S (2016) New insights into the phage genetic switch: effects of bacteriophage lambda operator mutations on DNA looping and regulation of PR, PL, and PRM. *J Mol Biol* 428(22):4438–4456. <https://doi.org/10.1016/j.jmb.2016.08.027>

- Li H, Lantz R, Du D (2019) Vibrational approach to the dynamics and structure of protein amyloids. *Molecules* 24(1):186. <https://doi.org/10.3390/molecules24010186>
- Louis-Jeune C, Andrade-Navarro MA, Perez-Iratxeta C (2012) Prediction of protein secondary structure from circular dichroism using theoretically derived spectra. *Proteins* 80(2):374–381. <https://doi.org/10.1002/prot.23188>
- Lowman HB, Bina M (1990) Temperature-mediated regulation and downstream inducible selection for controlling gene expression from the bacteriophage λ pL promoter. *Gene* 96(1):133–136. [https://doi.org/10.1016/0378-1119\(90\)90353-S](https://doi.org/10.1016/0378-1119(90)90353-S)
- Luviano A, Cruz-Castañeda R, Sánchez-Puig N, García-Hernández E (2019) Cooperative energetic effects elicited by the yeast Shwachman-Diamond syndrome protein (Sdo1) and guanine nucleotides modulate the complex conformational landscape of the elongation factor-like 1 (Efl1) GTPase. *Biophys Chem* 247:13–24. <https://doi.org/10.1016/j.bpc.2019.02.003>
- Macedo B, Sant'Anna R, Navarro S, Cordeiro Y, Ventura S (2015) Mammalian prion protein (PrP) forms conformationally different amyloid intracellular aggregates in bacteria. *Microb Cell Fact* 14(1):174. <https://doi.org/10.1186/s12934-015-0361-y>
- Malekian R, Jahanian-Najafabadi A, Moazen F, Ghavimi R, Mohammadi E, Akbari V (2019) High-yield production of granulocyte-macrophage colony-stimulating factor in *E. coli* BL21 (DE3) by an auto-induction strategy. *Iran J Pharm Res* 18(1):469–478
- Malekian R, Sima S, Jahanian-Najafabadi A, Moazen F, Akbari V (2019) Improvement of soluble expression of GM-CSF in the cytoplasm of *Escherichia coli* using chemical and molecular chaperones. *Protein Express Purif* 160:66–72. <https://doi.org/10.1016/j.pep.2019.04.002>
- Mansey MS, Ghareeb KA, Moghazy AN, Tawfik MM, Fouda MM, El Marzugi NA, Othman NZ, El Enshasy HA (2014) Glucose concentration affects recombinant interferon α -2b production in *Escherichia coli* using thermo-induction system. *J Appl Pharm Sci* 4:1–5. <https://doi.org/10.7324/JAPS.2014.40501>
- Margreiter G, Messner P, Caldwell KD, Bayer K (2008) Size characterization of inclusion bodies by sedimentation field-flow fractionation. *J Biotechnol* 138(3–4):67–73. <https://doi.org/10.1016/j.jbiotec.2008.07.1995>
- Mayer MP (2021) The Hsp70-chaperone machines in bacteria. *Front Mol Biosci* 8:694012. <https://doi.org/10.3389/fmolb.2021.694012>
- Mehta HM, Malandra M, Corey SJ (2015) G-CSF and GM-CSF in neutropenia. *J Immunol* 195(4):1341–1349. <https://doi.org/10.4049/jimmunol.1500861>
- Miller LM, Bourassa MW, Smith RJ (2013) FTIR spectroscopic imaging of protein aggregation in living cells. *Biochim Biophys Acta Biomembr* 1828(10):2339–2346. <https://doi.org/10.1016/j.bbamem.2013.01.014>
- Miller CA, Tucker WT, Meacock PA, Gustafsson P, Cohen SN (1983) Nucleotide sequence of the partition locus of *Escherichia coli* plasmid pSC101. *Gene* 24(2–3):309–315. [https://doi.org/10.1016/0378-1119\(83\)90091-4](https://doi.org/10.1016/0378-1119(83)90091-4)
- Monera OD, Kay CM, Hodges RS (1994) Protein denaturation with guanidine hydrochloride or urea provides a different estimate of stability depending on the contributions of electrostatic interactions. *Protein Sci* 3(11):1984–1991. <https://doi.org/10.1002/pro.5560031110>
- Morita MT, Tanaka Y, Kodama TS, Kyogoku Y, Yanagi H, Yura T (1999) Translational induction of heat shock transcription factor sigma32: evidence for a built-in RNA thermosensor. *Genes Dev* 13(6):655–665. <https://doi.org/10.1101/gad.13.6.655>
- Nicola NA, Metcalf D, Matsumoto M, Johnson GR (1983) Purification of a factor inducing differentiation in murine myelomonocytic leukemia cells. *J Biol Chem* 258(14):9017–9023. [https://doi.org/10.1016/S0021-9258\(18\)32158-6](https://doi.org/10.1016/S0021-9258(18)32158-6)
- Okamoto M, Nakai M, Nakayama C, Yanagi H, Matsui H, Noguchi H, Hara H (1991) Purification and characterization of three forms of differently glycosylated recombinant human granulocyte-macrophage colony-stimulating factor. *Arch Biochem Biophys* 286(2):562–568. [https://doi.org/10.1016/0003-9861\(91\)90080-3](https://doi.org/10.1016/0003-9861(91)90080-3)
- Olsson J, Paulsson J, Nordström K (2004) Effect of the CopB auxiliary replication control system on stability of maintenance of Par+ plasmid R1. *J Bacteriol* 186(1):207–211. <https://doi.org/10.1128/JB.186.1.207-211.2004>
- Overton TW (2014) Recombinant protein production in bacterial hosts. *Drug Discov Today* 19(5):590–601. <https://doi.org/10.1016/j.drudis.2013.11.008>
- Paek KH, Walker GC (1987) *Escherichia coli* dnaK null mutants are inviable at high temperature. *J Bacteriol* 169(1):283–290. <https://doi.org/10.1128/jb.169.1.283-290.1987>
- Pesarrodona M, Jauset T, Díaz-Riascos ZV, Sánchez-Chardi A, Beaulieu ME, Seras-Franzoso J, Sánchez-García L, Baltà-Foix R, Mancilla S, Fernández Y, Rinas U Jr, Schwartz S, Soucek L, Villaverde A, Abasolo I, Vázquez E (2019) Targeting antitumoral proteins to breast cancer by local administration of functional inclusion bodies. *Adv Sci (weinh)* 6(18):1900849. <https://doi.org/10.1002/advs.201900849>
- Peternel Š, Grdadolnik J, Gaberc-Porekar V, Komel R (2008) Engineering inclusion bodies for non-denaturing extraction of functional proteins. *Microb Cell Fact* 7(1):34. <https://doi.org/10.1186/1475-2859-7-34>
- Phue JN, Shiloach J (2004) Transcription levels of key metabolic genes are the cause for different glucose utilization pathways in *E. coli* B (BL21) and *E. coli* K (JM109). *J Biotechnol* 109(1–2):21–30. <https://doi.org/10.1016/j.jbiotec.2003.10.038>
- Remaut E, Stanssens P, Fiers W (1981) Plasmid vectors for high-efficiency expression controlled by the pL promoter of coliphage lambda. *Gene* 15(1):81–93. [https://doi.org/10.1016/0378-1119\(81\)90106-2](https://doi.org/10.1016/0378-1119(81)90106-2)
- Restrepo-Pineda S, Bando-Campos CG, Valdez-Cruz NA, Trujillo-Roldán MA (2019) Recombinant production of ESAT-6 antigen in thermoinducible *Escherichia coli*: the role of culture scale and temperature on metabolic response, expression of chaperones, and architecture of inclusion bodies. *Cell Stress Chaperon* 24:777–792. <https://doi.org/10.1007/s12192-019-01006-x>
- Restrepo-Pineda S, Pérez NO, Valdez-Cruz NA, Trujillo-Roldán MA (2021) Thermoinducible expression system for producing recombinant proteins in *Escherichia coli*: advances and insights. *FEMS Microbiol Rev* 45:fuab023. <https://doi.org/10.1093/femsre/fuab023>
- Rinas U, Hoffmann F, Betiku E, Estapé D, Marten S (2007) Inclusion body anatomy and functioning of chaperone-mediated in vivo inclusion body disassembly during high-level recombinant protein production in *Escherichia coli*. *J Biotechnol* 127(2):244–257. <https://doi.org/10.1016/j.jbiotec.2006.07.004>
- Rinas U, García-Fruitós E, Corchero JL, Vázquez E, Seras-Franzoso J, Villaverde A (2017) Bacterial inclusion bodies: discovering their better half. *Trends Biochem Sci* 1334:1–12. <https://doi.org/10.1016/j.tibs.2017.01.005>
- Rosano GL, Ceccarelli EA (2014) Recombinant protein expression in *Escherichia coli*: advances and challenges. *Front Microbiol* 5:172. <https://doi.org/10.3389/fmicb.2014.00172>
- Rosano GL, Morales ES, Ceccarelli EA (2019) New tools for recombinant protein production in *Escherichia coli*: A 5-year update. *Protein Sci* 28(8):1412–1422. <https://doi.org/10.1002/pro.3668>
- Sánchez-García L, Martín L, Mangués R, Ferrer-Mirallés N, Vázquez E, Villaverde A (2016) Recombinant pharmaceuticals from microbial cells: a 2015 update. *Microb Cell Fact* 15(1):33. <https://doi.org/10.1186/s12934-016-0437-3>
- Sandoval-Basurto EA, Gosset G, Bolívar F, Ramírez OT (2005) Culture of *Escherichia coli* under dissolved oxygen gradients

- simulated in a two-compartment scale-down system: Metabolic response and production of recombinant protein. *Biotechnol Bioeng* 89(4):453–463
- Schwanke RC, Renard G, Chies JM, Campos MM, Junior ELB, Santos DS, Basso LA (2009) Molecular cloning, expression in *Escherichia coli* and production of bioactive homogeneous recombinant human granulocyte and macrophage colony stimulating factor. *Int J Biol Macromol* 45(2):97–102. <https://doi.org/10.1016/j.ijbmac.2009.04.005>
- Shiloach J, Rinas U (2009) Glucose and acetate metabolism in *E. coli* – system level analysis and biotechnological applications in protein production processes. In: Lee SY (ed) *Systems Biology and Biotechnology of Escherichia coli*. Springer, Dordrecht. https://doi.org/10.1007/978-1-4020-9394-4_18
- Singh SM, Panda AK (2005) Solubilization and refolding of bacterial inclusion body proteins. *J Biosci Bioeng* 99(4):303–310. <https://doi.org/10.1263/jbb.99.303>
- Singh A, Upadhyay V, Panda AK (2015) Solubilization and refolding of inclusion body proteins. *Methods Mol Biol* 1258:283–291. https://doi.org/10.1007/978-1-4939-2205-5_15
- Singh A, Upadhyay V, Singh A, Panda AK (2020) Structure-function relationship of inclusion bodies of a multimeric protein. *Front Microbiol* 11:876. <https://doi.org/10.3389/fmicb.2020.00876>
- Singha TK, Gulati P, Kumar S (2018) Nonconventional induction strategies for production of recombinant human tumor necrosis factor- α in *Escherichia coli*. *J App Biol Biotechnol* 6:23–27. <https://doi.org/10.7324/JABB.2018.60105>
- Singhvi P, Saneja A, Srichandan S, Panda AK (2020) Bacterial inclusion bodies: a treasure trove of bioactive proteins. *Trends Biotechnol* 38(5):474–486. <https://doi.org/10.1016/j.tibtech.2019.12.011>
- Terol GL, Gallego-Jara J, Martínez RAS, Vivancos AM, Díaz MC, Puente TD (2021) Impact of the expression system on recombinant protein production in *Escherichia coli* BL21. *Front Microbiol* 12:682001. <https://doi.org/10.3389/fmicb.2021.682001>
- Thomson CA, Olson M, Jackson LM, Schrader JW (2012) A simplified method for the efficient refolding and purification of recombinant human GM-CSF. *PLoS ONE* 7(11):e49891. <https://doi.org/10.1371/journal.pone.0049891>
- Trapnell BC, Inoue Y, Bonella F, Morgan C, Jouneau S, Bendstrup E, Campo I, Papis SA, Yamaguchi E, Cetinkaya E, Ilkovich MM, Kramer MR, Veltkamp M, Kreuter M, Baba T, Ganslandt C, Tarnow I, Waterer G, Jauhikainen T, IMPALA Trial Investigators (2020) Inhaled Molgramostim therapy in autoimmune pulmonary alveolar proteinosis. *N Engl J Med* 383(17):1635–1644. <https://doi.org/10.1056/NEJMoa1913590>
- Trujillo-Roldán MA, Peña C, Ramírez OT, Galindo E (2001) Effect of oscillating dissolved oxygen tension on the production of alginate by *Azotobacter vinelandii*. *Biotechnol Prog* 17(6):1042–1048. <https://doi.org/10.1021/bp010106d>
- Upadhyay AK, Murmu A, Singh A, Panda AK (2012) Kinetics of inclusion body formation and its correlation with the characteristics of protein aggregates in *Escherichia coli*. *PLoS ONE* 7:e33951. <https://doi.org/10.1371/journal.pone.0033951>
- Upadhyay V, Singh A, Jha D, Singh A, Panda AK (2016) Recovery of bioactive protein from bacterial inclusion bodies using trifluoroethanol as solubilization agent. *Microb Cell Fact* 15(1):1–13. <https://doi.org/10.1186/s12934-016-0504-9>
- Valdez-Cruz NA, Caspeta L, Pérez NO, Ramírez OT, Trujillo-Roldán MA (2010) Production of recombinant proteins in *E. coli* by the heat inducible expression system based on the phage lambda *pL* and/or *pR* promoters. *Microb Cell Fact* 9:18. <https://doi.org/10.1186/1475-2859-9-18>
- Valdez-Cruz NA, Ramírez OT, Trujillo-Roldán MA (2011) Molecular responses of *E. coli* caused by heat stress and recombinant protein production during temperature induction. *Bioeng Bugs* 2(2):105–110. <https://doi.org/10.4161/bbug.2.2.14316>
- Valdez-Cruz NA, Reynoso-Cereceda GI, Pérez-Rodríguez S, Restrepo-Pineda S, González-Santana J, Olvera A, Trujillo-Roldán MA (2017) Production of a recombinant phospholipase A2 in *Escherichia coli* using resonant acoustic mixing that improves oxygen transfer in shake flasks. *Microb Cell Fact* 16(1):129. <https://doi.org/10.1186/s12934-017-0746-1>
- Vázquez-Fernández E, Alonso J, Pastrana MA, Ramos A, Stitz L, Vidal E, Dynin I, Petsch B, Silva CJ, Requena JR (2012) Structural organization of mammalian prions as probed by limited proteolysis. *PLoS ONE* 7(11):e50111. <https://doi.org/10.1371/journal.pone.0050111>
- Villaverde A, Benito A, Viaplana E, Cubarsi R (1993) Fine regulation of c1857- controlled gene expression in continuous culture of recombinant *Escherichia coli* by temperature. *Appl Environ Microb* 59(10):3485–3487. <https://doi.org/10.1128/aem.59.10.3485-3487.1993>
- Villaverde A, García-Fruitós E, Rinas U, Seras-Franzoso J, Kosoy A, Corchero JL, Vazquez E (2012) Packaging protein drugs as bacterial inclusion bodies for therapeutic applications. *Microb Cell Fact* 11(1):1–5. <https://doi.org/10.1186/1475-2859-11-76>
- Walsh G (2018) Biopharmaceutical benchmarks 2018. *Nat Biotechnol* 36:1136–1145. <https://doi.org/10.1038/nbt.4305>
- Walter MR, Cook WJ, Ealick SE, Nagabhushan TL, Trotta PP, Bugg CE (1992) Three dimensional structure of recombinant human granulocyte-macrophage colony stimulating factor. *J Mol Biol* 224(4):1075–1085. [https://doi.org/10.1016/0022-2836\(92\)90470-5](https://doi.org/10.1016/0022-2836(92)90470-5)
- Wicks IP, Roberts AW (2016) Targeting GM-CSF in inflammatory diseases. *Nat Rev Rheumatol* 12(1):37–48. <https://doi.org/10.1038/nrrheum.2015.161>
- Williams DC, Van Frank RM, Muth WL, Burnett JP (1982) Cytoplasmic inclusion bodies in *Escherichia coli* producing biosynthetic human insulin proteins. *Science* 215(4533):687–689. <https://doi.org/10.1126/science.7036343>
- Wingfield P, Graber P, Moonen P, Craig S, Pain R (1988) The conformation and stability of recombinant-derived granulocyte-macrophage colony stimulating factors. *Eur J Biochem* 173(1):65–72. <https://doi.org/10.1111/j.1432-1033.1988.tb13967.x>
- Wittmann C, Weber J, Betiku E, Krömer J, Böhm D, Rinas U (2007) Response of fluxome and metabolome to temperature-induced recombinant protein synthesis in *Escherichia coli*. *J Biotechnol* 132(4):375–384. <https://doi.org/10.1016/j.jbiotec.2007.07.495>
- Wu C, Biancalana M, Koide S, Shea JE (2009) Binding modes of thiopyran-T to the single-layer β -sheet of the peptide self-assembly mimics. *J Mol Biol* 394(4):627–633. <https://doi.org/10.1016/j.jmb.2009.09.056>
- Yamamori T, Ito K, Nakamura Y, Yura T (1978) Transient regulation of protein synthesis in *Escherichia coli* upon shift-up of growth temperature. *J Bacteriol* 134(3):1133–1140. <https://doi.org/10.1128/jb.134.3.1133-1140.1978>
- Yano R, Nagai H, Shiba K, Yura T (1990) A mutation that enhances synthesis of sigma 32 and suppresses temperature-sensitive growth of the rpoH15 mutant of *Escherichia coli*. *J Bacteriol* 172(4):2124–2130. <https://doi.org/10.1128/jb.172.4.2124-2130.1990>
- Yura T (2019) Regulation of the heat shock response in *Escherichia coli*: history and perspectives. *Genes Genet Syst* 94:103–108. <https://doi.org/10.1266/ggs.19-00005>
- Zhang F, Weng D, Su Y, Yin C, Shen L, Zhang Y, Zhou Y, Li Q, Hu Y, Li H (2020) Therapeutic effect of subcutaneous injection of low dose recombinant human granulocyte-macrophage colony-stimulating factor on pulmonary alveolar proteinosis. *Respir Res* 21(1):1. <https://doi.org/10.1186/s12931-019-1261-1>

Publisher's note Springer Nature remains neutral with regard to jurisdictional claims in published maps and institutional affiliations.